Tetsuo Asakura • Thomas Miller
Editors

Biotechnology of Silk

Springer

Editors
Tetsuo Asakura
Department of Biotechnology
Tokyo University of Agriculture
and Technology
Koganei, Tokyo
Japan

Thomas Miller
Department of Entomology
University of California – Riverside
Riverside, CA
USA

ISSN 2211-0593
ISBN 978-94-007-7118-5
DOI 10.1007/978-94-007-7119-2
Springer Dordrecht Heidelberg New York London

ISSN 2211-0607 (electronic)
ISBN 978-94-007-7119-2 (eBook)

Library of Congress Control Number: 2013951649

Printed on acid-free paper

Springer is part of Springer Science+Business Media (www.springer.com)

Chapter 12
Silk and Web Synergy: The Merging of Material and Structural Performance

Steven W. Cranford, Nicola M. Pugno, and Markus J. Buehler

Abstract Millions of years of evolution have adapted spider silks to achieve a range of functions, including the well-known capture of prey, with efficient use of material. From a materials perspective, the exceptional mechanical properties of self-assembling silk biopolymers have been extensively explored, both experimentally and in computational investigations. Yet few studies account for the structural function of silk within the web itself. Recently, a series of investigations have been conducted to examine structure-function relationships across different length scales in silk, ranging from atomistic models of protein constituents to the spider web architecture. Here, through theoretical and computational models, we attempt to reconcile the unique mechanical behavior of spider silk (*i.e.*, material) with the performance of the web itself (*i.e.*, structure), and elucidate the intimate and synergistic relationship between the two – the ultimate merging of material and structure. Particularly, we review recent analyses that considered an entire web structure subject to load, as well as the critical anchorage that secures the

S.W. Cranford
Laboratory of Nanotechnology in Civil Engineering, Department of Civil and Environmental Engineering, Northeastern University, 403 Snell Engineering, 360 Huntington Avenue, Boston, MA 02115, USA
e-mail: s.cranford@neu.edu

N.M. Pugno (✉)
Laboratory of Bio-Inspired and Graphene Nanomechanics, Department of Civil, Environmental and Mechanical Engineering, Università di Trento, via Mesiano, 77, I-38123 Trento, Italy

Center for Materials and Microsystems, Fondazione Bruno Kessler, Via Sommarive 18, 38123 Povo (Trento), Italy
e-mail: nicola.pugno@unitn.it

M.J. Buehler (✉)
Laboratory for Atomistic and Molecular Mechanics (LAMM), Department of Civil and Environmental Engineering, Massachusetts Institute of Technology, 77 Massachusetts Avenue, Cambridge, MA 02139, USA
e-mail: mbuehler@MIT.EDU

T. Asakura and T. Miller (eds.), *Biotechnology of Silk*, Biologically-Inspired Systems 5,
DOI 10.1007/978-94-007-7119-2_12,

web to its (uncertain) environment. Beyond assessment of simple performance, we derive the theoretical basis for the underlying mechanics (through quantized fracture mechanics and the theory of multiple peeling, respectively). As such, the results can be translated to engineered structures in general, beyond the particular case of spider silks and webs. Interestingly, in both cases (web fracture and anchorage failure), the extreme hyperelasticity – *i.e.* elastic stiffening under large extension – benefits structural performance, in contrast to typical engineering practice (wherein large deformation is typically avoided). The spider web is a highly adapted system where both material and hierarchical structure across all length-scales is critical for its functional properties.

Keywords Silk • Webs • Multiscale • Structure-function • Modeling • Nano-to-macro • Materiomics • Detachment • Multiple peeling • Fracture • Quantized fracture mechanics • Robustness

12.1 Introduction: Biomimicry and Stealing Ideas from Silk

Looking around the natural world, it is clear that Nature presents an array of materials that provide a multitude of functions. The elasticity of blood vessels, the toughness of bone, and the protection of nacre illustrate the *apropos* of Nature's material selection (Gosline et al. 1999; Gao et al. 2003; Aizenberg et al. 2005; Vollrath 1992; Kamat et al. 2000) and synergistic relationships between *material* and *structure*. Similarly, spider webs are fascinating examples of natural structural engineering essential for an animal's survival (Hansell 2005; Tarakanova and Buehler 2012a). In parallel, natural web architectures provide an inspiration to structural engineers (Carpinteri and Pugno 2008) while matching the remarkable properties of silk fibers presents a challenge to materials scientists (Bosia et al. 2010; Pugno 2007). That being said, recent work suggests that the *separate* consideration of structure and material is insufficient – material properties govern the structure and *vice versa*, creating heightened functionality through synergistic interactions (Agnarsson and Blackledge 2009; Sensenig et al. 2010; Opell and Bond 2001). For example, a spider may vary the properties of a piece of thread depending on its placement in the web (Boutry and Blackledge 2009). Complete understanding of the silk/web system, therefore, requires the merging of material and structural performance.

Spider silks, ranging from the protein sequence (Lefevre et al. 2007) to the geometry of a web (Vollrath and Mohren 1985), have intrigued scientists as a highly adapted system (Vollrath 2010), well-known for its exemplary mechanical properties (Agnarsson et al. 2010; Du et al. 2006; Shao and Vollrath 2002; Omenetto and Kaplan 2010; Ko et al. 2002). The evolutionary demands placed on spiders (Lewis 2006) are reflected in the design of their webs, both structurally and from a materials perspective (Cranford et al. 2012). Spider silk is an ideal herald of Nature's evolutionary success, surpassing high energy-absorbing materials such as Kevlar and carbon fiber, and providing an extremely light-weight alternative (Gosline et al. 1999; Vollrath 2010; Agnarsson et al. 2010; Swanson et al. 2009).

A combination of high tensile strength on par with steel (at 1–2 GPa (Swanson et al. 2009)) and extensibility (up to 60 % maximum strain (Swanson et al. 2009)) result in superior toughness, and exceeding performance when normalized by its density. Spiders utilize these unique material properties to construct geometrically organized web structures which serve a variety of purposes. Indeed, beyond catching insects as prey, spider silk has evolved to fulfil multiple functions such as construction of egg sacks and cocoons (Rammensee et al. 2008), making it one of the most versatile known materials (Shao and Vollrath 2002; Vollrath et al. 1996). Interest to understand this material (Aoyanagi and Okumura 2010; Ko and Jovicic 2004; Alam et al. 2007) has led to recent studies at the molecular scale (Keten et al. 2010; Keten and Buehler 2010a), as well as the mechanical characteristics of web-like structures (Aoyanagi and Okumura 2010; Ko and Jovicic 2004; Alam et al. 2007; Alam and Jenkins 2005). However, from a mechanistic perspective, it still remains relatively unknown how silk's distinct material behaviour may benefit the structural integrity and performance of a spider web. From another perspective, would webs be just as efficient if they were constructed out of steel? Or perhaps nylon? Ultimately we ask: what can be learned from spider silk and webs?

A common research thrust is the field of *biomimicry* – that is, using ideas from Nature as a design guide to solve a technological problem. Through continuous processes of trial and error and self-selectivity, Nature has successfully refined living organisms, processes, and materials, acting as both an astute materials scientist and efficient engineer. Common examples include biomaterials (*e.g.*, surgical implants that mimic the necessary tissues) or self-cleaning hydrophobic surfaces based on a lotus leaf. More recently, materials scientists and engineers have looked at biological materials and systems at reduced scales, to probe the toughness of spider silk and mollusk nacre, the structure of sea sponges, or the adhesion of gecko feet. The findings have motivated the development of *de novo* material systems for various applications. That being said, one of the disciplines that Nature currently has little impact is structural engineering. While a few architects have incorporated biomimicry for aesthetic purposes (Knippers and Speck 2012), the underlying structures are bound to man-made (and designed) structural elements – trusses, girders, beam-columns joints, moment frames, etc. *Need this be the case*?

At first glance, the design strategies of biological materials and systems are neither immediately applicable to, nor compatible with the design of new engineered structures, since there are constraining differences in scale, constructability, and function. The transfer of ideas from biology, however, is not limited to the ultimate form and function of a biological system – we are not interested in spider silk such that we can swing from skyscrapers like Spiderman (although it would be an interesting proposal!). Rather, out motivation lies in translating the basic mechanics of spider silks and webs to potential engineered designs. This requires robust understanding of the mechanics and physics behind observation. In order to exploit the full potential of biomimicry, we must move beyond simple *replication* of biological systems, and successfully develop pathways for the extension of Nature's principles. Indeed, many engineers may not know the most relevant biological phenomena for any given design problem – but the underlying physics and mechanics is constant. A holistic knowledge of biological materials and systems

(an emerging field known as *materiomics* (Cranford and Buehler 2012)) offers a unique opportunity to understand how complex materials science and engineering principles arise routinely in Nature.

This field defines biomimetics – using ideas from nature to further technology – or, more colloquially, "... *the technological outcome of the act of borrowing or stealing ideas from Nature*" (Vincent 2001). Biomimetics, however, is extending beyond the simple "stealing" of ideas, and evolving to a more didactic role – *i.e. learning* ideas from Nature. The difference lies not just in the abstraction of useful ideas (the invention of Velcro by the observation of sticking plant burrs is a popular example) but also in the detailed and mechanistic understanding of the processes involved. Instead, we should look to Nature and biological systems (nay, models), to serve a technical application of practical purpose. The more this application deviates from the biological system, the more basic the analysis has to be in order to generate useful (practical) knowledge and understanding (see Fig. 12.1). The general concept is that the further down one can move from the natural origin, the more general and therefore more powerful the concept will be. The goal is the shift from total mimicry (stealing) to an understanding of the process at its basic level (abstraction), defining that process from an analytical perspective (mechanics and physics) and then exploiting the physical phenomena to our own ends. Investigations and studies discussed can be assigned to such categorizations.

In this chapter, we attempt to reconcile multi-scale studies of silk/webs spanning lengths from Ångstroms to centimeters, from the amino acid sequence defining silk components to an atomistically-derived spider web model, with the aim to bridge varying levels of hierarchy to elucidate the fundamental mechanisms by which components at each scale contributes to ultimate structural behavior. Emphasis is given to theoretical descriptions and derivations of the phenomena. As such, the assumptions utilized to "bridge scales" (such as neglecting the idiosyncratic self-assembly of silk fibers) become secondary to the idealized model performance, and thus a useful engineering tool. We hence exploit silk/web synergy as a platform for mechanistic discovery.

A fundamental understanding of structure-function relationships across different length scales of silk is required and forms an excellent model system to apply the principles of *materiomics* – involving multiscale simulation, theory, and experiment – to span all scales and arrive at a model that describes material function of the entire system as the interplay of a material's building blocks (Spivak et al. 2011). Thus, while out ultimate motivation is structural (*i.e.*, web) performance, we first need to understand the performance of our construction materials – namely the general constitutive behaviour of spider silk.

12.2 A Complex Biological Material

The distinct behaviour of silk, like other biological systems, is established by a hierarchical configuration (Ko et al. 2002; Keten et al. 2010; Keten and Buehler 2010a; Vepari and Kaplan 2007; Swanson et al. 2007), which is itself dictated

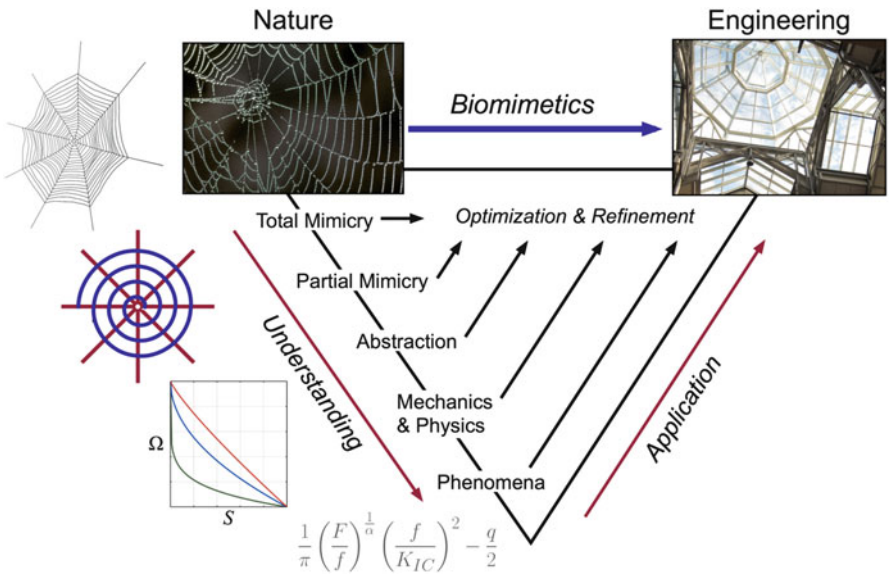

Fig. 12.1 A biomimetic "map" to illustrate the idea that the more abstract a concept is, the more adaptable it is within another discipline, applied specifically here to spider silk/webs. While spider webs provide an intriguing natural structure and silk itself is undoubtedly a high performance material, we do not study silk/webs to swing from the sky like Spiderman. Rather than mimicry, we are interested in the underlying phenomena, which can be applied to engineered structures in general. This requires a multistep analysis, wherein we progress from partial mimicry (*e.g.*, idealized silk and web models) to systematically probe the general mechanics and physics that govern system performance. In effect, we do not need to replicate the behavior of silk and webs with 100 % accuracy, but rather only reflect the key (but unknown) behaviors and relationships (Adapted from Vincent 2001 and Cranford and Buehler 2012)

by the proteins that constitute silk. Proteins play a critical role as the building blocks of many complex hierarchical biological materials (Omenetto and Kaplan 2010; Rammensee et al. 2008; Vepari and Kaplan 2007; Fratzl and Barth 2009; Buehler and Yung 2009). While all proteins can be described by a sequence of only 20 available amino acids, the diversified functionality of protein-based materials is often a result of variations in structure, rooted in the molecular composition and expanding the material design space to incorporate multiple levels (Buehler and Yung 2009; Buehler 2010; Sen and Buehler 2011). The variable geometric and topological conformations (*i.e.*, folding) of proteins is the fundamental basis for creation of the first hierarchies of biological materials. The introduction of "folded" variations can be through of as a mechanism to extend the possible "design space" (*e.g.*, achievable properties and functions) with a limited number of building blocks (*e.g.*, amino acids). The intrinsic flexibility and entropically governed nature of protein materials permit multiple variations in structure (*qua* function) with nominal required changes in sequence. The other side of the coin, of course, is that knowledge of sequence alone is not sufficient to "create" synthetic silk, requiring ingenious methods to replicate assembly conditions.

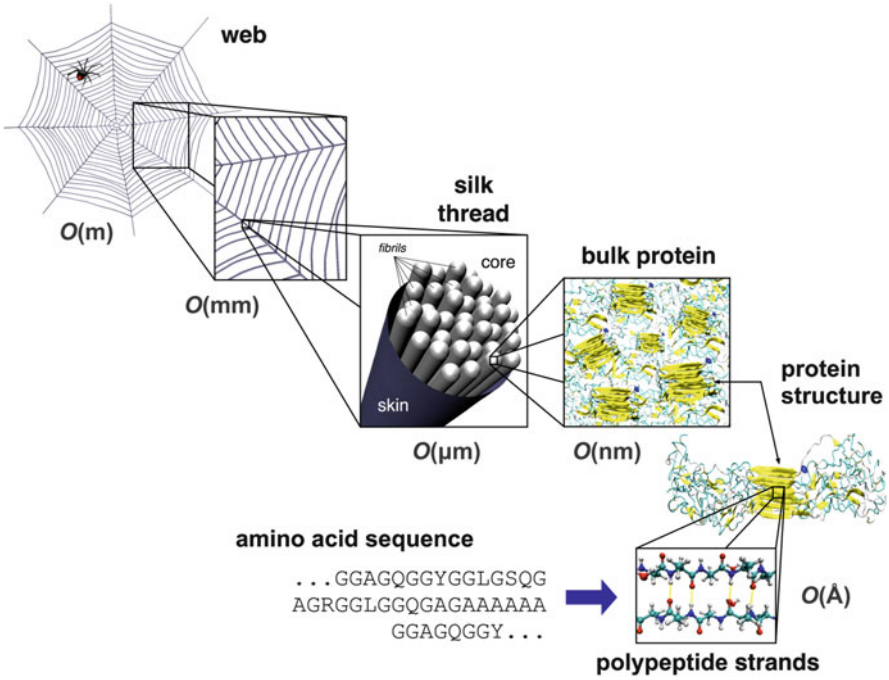

Fig. 12.2 Schematic of the hierarchical spider silk/web structure that ranges from nano (Ångstrom) to macro (millimeters, meters). Displays key structural features of silk, including the peptide sequence (chemical structure) found at the hydrogen bonded β-strands (Ångstrom), the secondary protein structure consisting of β-sheet nanocrystals embedded in a softer semi-amorphous phase (nanometers), bulk protein assembly of poly-crystalline components which assembly into microscopic silk fibrils (nanometers), themselves bundled into larger silk fibers/threads (in a skin-core arrangement; micrometers), and finally the web-structure itself (which consists of multiple silk types; millimeters and meters). The focus of this chapter is the representation of the molecular structure of spider silk through a macroscale investigation of a complete spider web and its behavior

Spider silk is an excellent demonstration of a biological protein fiber where the hierarchical structure – exhibiting weak hydrogen bonding at its core – regulates material behavior on multiple length scales. While spider silk is employed in a myriad of functions, from wrapping prey to lining retreats (Foelix 1996; Vollrath 1999), the most widely studied silk, and the focus of this chapter, is dragline silk (Vollrath et al. 1996; Vollrath 1999), which functions to provide a stable framework in webs (Gosline et al. 1999). It is composed of β-sheet nanocrystals interspersed within less orderly amorphous domains, where the underlying molecular structure is dominated by weak hydrogen bonding. The hierarchies in dragline silk's material composition are illustrated in Fig. 12.2.

12.2.1 Molecular Structure and Mechanics of Silk

The analysis of material properties at multiple scales is a crucial issue in understanding biological materials, as their structure changes with hierarchical level (and thus length-scale), and therefore most material properties are strongly dependent on the scale of observation. Multi-scale experimental and simulation analyses are the key to improve our systematic understanding of how structure and properties are linked. Typically this is achieved from a *bottom-up* approach, linking more sophisticated lower length-scale parameters, which form the building blocks of the system at that level, to coarser, larger length-scales. Purely "bottom-up" approaches, however, are incomplete if they lack the interpretation of large-scale behavior to small-scale phenomena, an iterative "nano-to-macro-to-nano" paradigm. Full stratification of different levels of hierarchy using such analysis develops a powerful feedback loop where the bottom-up modeling approach catalyzes the insights we gain at each layer of the material ladder, with the possibility of controlling properties at multiple scales simultaneously, and to examine their effect on system function. Undoubtedly, mechanical performance provides a means to characterize behaviors and properties analogous to engineering practices – we may want to mimic silk to attain a high-performance synthetic fiber, for example, and not a web-like meshwork to capture flies.

Silk's lowest level of hierarchy is rooted in its primary protein structure, defined by a sequence of amino acid residues, which is responsible for subsequent folding mechanisms that leads to the defining molecular structure. The focus here is given to dragline silk, produced from the spider's major ampullate (MA) silk glands, with a unique and well researched constitutive behaviour, and important as a structural element in webs (Vollrath 2000). Even so, while most spiders produce some form of dragline silk, the specific material properties vary among different evolutionary species (Opell and Bond 2001; Swanson et al. 2006, 2009; Elices et al. 2009; Vollrath and Selden 2007). Even among orb web weaving spiders (in which dragline silk serves a similar purpose) the material properties of dragline silk vary by more than 100 %, and across all spiders toughness varies over 20-fold in species examined to date (Agnarsson et al. 2010). Another key silk type within the web is the sticky capture silk, made of a viscid silk that originates from flagelliform glands (Vollrath 2000; Kohler and Vollrath 1995; Lin and Sobek 1998) and used to form the spiral threads in a web. Both viscid and dragline silks express a stiffening stress–strain behaviour, where viscid silk is approximately ten times more extensible than dragline silk (Vollrath 2000; Kohler and Vollrath 1995). Dragline silk, however, is the most well researched silk with theoretical (Termonia 1994), computational (Keten and Buehler 2010a), and experimental (Du et al. 2006) studies across a multitude of scales elucidating its mechanical behaviour.

Residue segments in dragline silks form secondary structures, including crystalline β-sheets, 3_1-helices and so-called β-turns (Heim et al. 2010). The chemical bonding within these structures determines the material properties of each, where dense hydrogen bonds (H-bonds) compose the stiffer crystals, while dispersed

H-bonds join together extendable helices and β-turns. Three dimensional arrangements of the secondary structures form a higher-order protein structure, where β-sheet crystals are embedded in the amorphous meshwork of less orderly structures. Protein chains combine into silk fibrils which bundle together into the fibers forming threads in the web of a spider.

To study the link between chemical composition, structure and mechanical behavior at the molecular scale, a full atomistic model was created using a bottom-up molecular dynamics approach to identify native structures of the silk protein (Keten et al. 2010), starting from primary structures of silk proteins with the amino acid sequence of the *Nephila clavipes* dragline MaSp1 protein (Keten and Buehler 2010b) (in one-letter amino-acid code):

```
...GGAGQGGYGGLGSQGAGRGGLGGQGAGAAAAAAGGAGQGGYGGLGSQGAGR
   GGLGGQGAG...
```

From this sequence, the starting configuration of the composite protein structure was constructed, also accounting for the natural silk spinning process that involves elongational flow and alignment of protein chains due to mechanical force (Rammensee et al. 2008; Keten et al. 2010; Keten and Buehler 2010b; Ma and Nussinov 2002). Replica exchange molecular dynamics (Sugita and Okamoto 1999), REMD, an enhanced sampling method to explore a much longer timescale than accessible to conventional molecular dynamics, was employed as a means to predict native structures, by overcoming energy barriers and local minima (Feig et al. 2004). Computational results were validated with experimental data by comparing Ramachandran plots, showing that the computational predicts yield excellent results when compared to empirical analyses (van Beek et al. 2002; Kummerlen et al. 1996). Further details can be found in the original paper (Keten et al. 2010). Analysis of the resulting structures showed that the poly-alanine region and adjacent poly-glycine-alanine segments formed a stiff orderly cross-linking domain of the β-sheet crystal, embedded in a semi-amorphous matrix formed by two surrounding GGX repeat regions. In fact, this model first identified the secondary structure composition of the amorphous regions, showing a lack of alpha-helix conformations, but rather a disorderly mixture of structures resembling 3_1-helices and β-turns, supporting a series of earlier experimental investigations (van Beek et al. 2002; Jelinski 1998; Holland et al. 2008; Jenkins et al. 2010).

Silk's extraordinary properties on the macroscopic scale ultimately stem from the balance of strength and extensibility at the molecular scale (molecular deformation depicted in Fig. 12.3). To assess the function of different protein domains molecular-level deformation mechanisms of the protein composite were examined (Keten et al. 2010). These studies revealed that the balance is achieved through the combination of distinct secondary structure units in silk protein, where the interplay of the two constituent domains characterizes the nanoscale deformation mechanisms of the emerging nanocomposite structure. It was seen that initially, the amorphous domain unfolds, as H-bonds break and the β-turn content decreases. Beta turns within the

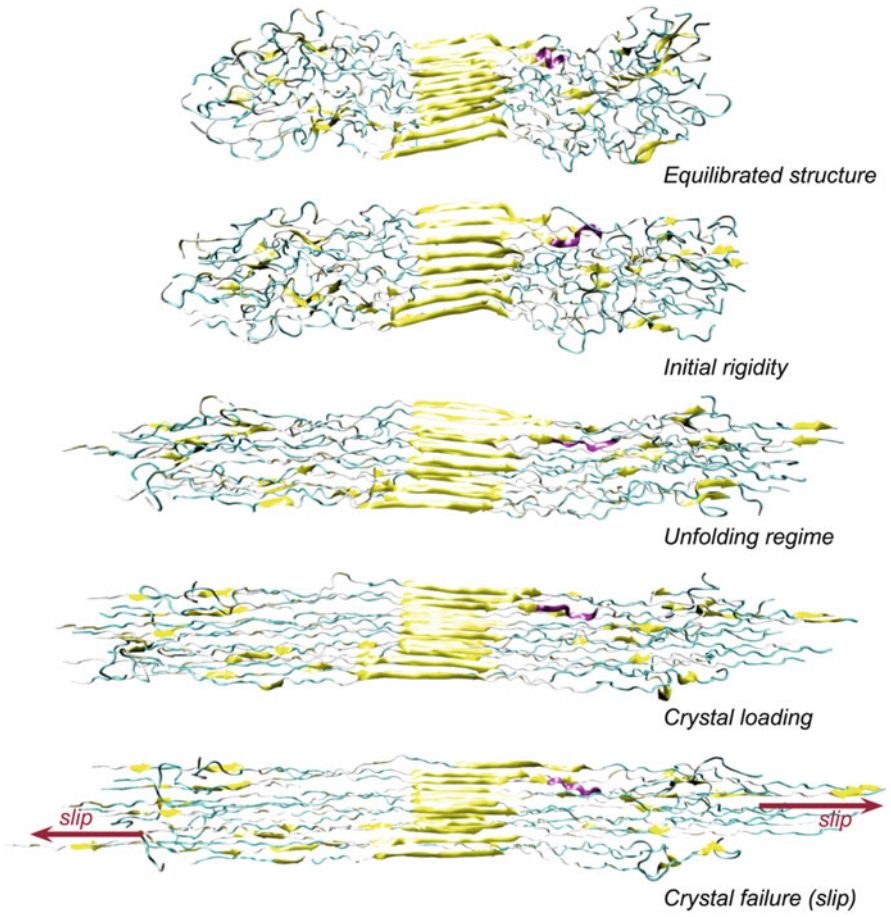

Fig. 12.3 Deformation of a macromolecular dragline silk protein structure. The figure illustrates the general stretching behavior of the amorphous domains and crystals under shear forces (loading of alternating strands) for MaSp2. *Top to bottom* reflects the time sequence of events during the REMD stretching simulations (Keten and Buehler 2010a). Four regimes of deformation are expressed: initial rigidity (due to weakly bonded amorphous region), entropic unfolding after initial yield, transfer of load to the crystalline domain (stiffening), and finally, crystal failure (slip). As evident from the time sequence of snapshots, amorphous domains stretch significantly, and a transition from turn to β-sheet structures is observed. A key observation is that failure of the system happens by sliding of strands with respect to each other upon breaking of the hydrogen bonds and side-chain contacts in the crystalline domain. This typically occurs at the interface region with solvent at the boundary of the crystal, leaving part of the crystal intact even after failure of the structure (Adapted from Keten and Buehler 2010a)

amorphous domains provide *hidden length*, leading to the great extensibility and toughness observed in silk. A comparison between a series of native structures displayed an enhanced initial stiffening regime and an increase in extensibility for structures with higher turn content (Keten et al. 2010). As the structure is further extended, β-sheet crystals form in the amorphous domains, bearing the exerted stress. Stiffening occurs as covalent bonds extend and hydrogen bonds rupture in the amorphous regions. Failure occurs as hydrogen bonds break in the crystalline regions, which triggers the sliding of β-sheet strands. This coherent interaction among different domains (Nova et al. 2010) within the silk protein results in a nonlinear constituent behavior of silk comparable to experimental studies (Du et al. 2006) of silk threads, achieving high strengths from the stiff crystal components, and improved extensibility and toughness resultant from constituents of the amorphous region.

The performance of the different sized crystals was also compared in pull out simulations, where a middle strand was loaded with a constant pulling velocity. In small crystals, a stick–slip motion was observed as hydrogen bonds broke and reformed. The self-healing ability of smaller crystals owing to the continuous reformation of hydrogen bonds protects the crystals from catastrophic failure as hydrogen bonds are shielded from exposure to water which facilitates rupture. Thus, the cooperative assembly of weak hydrogen bonds shaping geometry at the nanoscale exemplifies a hierarchical bridging mechanism between the Ångstrom and the molecular scale.

For our purposes, the characterization of silk behavior ends at the molecular level, but that is not the entire story (Tarakanova and Buehler 2012a). The silk protein is inevitably spun by spider spiggots and spinnerets, into larger order systems, forming nanoscale fibrils, which are themselves bundled into microscale fibers or threads (Vollrath and Knight 2001), as depicted in Fig. 12.2. This process is nontrivial, demonstrated by previous attempts to produce synthetic fibers that matched the performance of natural silks ultimately failed in their endeavors to "copy Nature" (Vollrath et al. 2011; O'Brien et al. 1998; Lazaris et al. 2002). Moreover, there are studies of individual fibril behavior (to determine their critical length scale (Giesa et al. 2011), for example) as well as the structure and mechanical implications of the fiber (Agnarsson et al. 2010; Du et al. 2006; Brown et al. 2012) (with a so-called skin-core arrangement of fibrils (Frische et al. 1998; Li et al. 1994; Poza et al. 2002)). Mechanisms at this scale – such as *supercontraction* (Elices et al. 2011; Agnarsson et al. 2009; Liu et al. 2005; Guinea et al. 2003; Shao and Vollrath 1999) – are critical to the full understanding of spider silk. That being said, experimental explorations of the mechanics of silk threads have indicated a constitutive (*e.g.*, stress–strain) response that is remarkable similar to the behavior of the molecular model discussed here (Agnarsson et al. 2010; Du et al. 2006). It appears Nature has successfully developed a protocol to "scale-up" the protein response. Thus, we have sufficient information to develop a general silk material model – not necessarily bound to a particular silk – but expressing the same regimes of behavior, which can be directly related to molecular response.

12.2.2 The "Model" Behavior of Silk

The natural variability in mechanical behavior makes it difficult to define "silk" with a single set of parameters. Some view the use of molecular mechanics and dynamics as largely inappropriate for modeling the highly nonlinear viscoelastic properties of silks (Vollrath et al. 2011), limited to calculating a linear elastic modulus of a generic silk polymer within the variability range of experimental observations (Vollrath and Porter 2009). In a similar vein, micro-mechanics based on continuum tools such as finite element methods are limited in delineating structural mechanisms if incorrect nonlinear viscoelastic parameters or morphologies are used within the model (Cetinkaya et al. 2011). Indeed, simpler polymer models are able predict a modulus, yield stress, and failure initiation guides based on generic observations on synthetic polymer parameters and morphologies such as cohesive energy density of molecular interactions, and such structure–property rules can be applied very successfully to native silks (Vollrath and Porter 2009; Porter et al. 2005; Porter and Vollrath 2007, 2009). Such models have been extended to encapsulate the storage of mechanical energy by ordered ("crystal") domains and the dissipation of energy by disordered ("amorphous") domains (Vollrath and Porter 2006, 2009). Successful in mapping nonlinear silk property profiles to an envelope of "representative" curves (Vollrath et al. 2011; Vollrath and Porter 2006), such methods reciprocally complement nanomechanical studies.

The prime advantage of atomistic modeling lies in the fact that structural transformations and failure mechanisms can be explicitly *observed* and/or *discovered* from the trajectories obtained from stretching simulations of the spider silk assemblies. For example, the amorphous domains stretch significantly with applied force, and a transition from turn to β-sheet structures can be quantified. A key observation is that failure of the system happens by sliding of β-strands with respect to each other, which can occur only upon breaking of the H-bonds in the crystalline domain, an observation only able to be fully captured by full atomistic modeling. Close investigation unveils a number of generic interactions between silk properties and molecular structures that can be generalized as "representative behavior". For example, the force-extension profiles of the modeled silk sequences depict a distinct characteristic curve that can be described by four regimes:

1. Initial rigidity until a yield point; the semi-amorphous domains homogeneously stretch and bear load until the disordered H-bonded structure fails;
2. The entropic unfolding regime where the associated 3_1-helices and β-turns begin to rupture resulting in a high extensibility (hidden length) under relatively low stress;
3. Severe stiffening as aligned amorphous strands begin to form addition H-bonds, and load directly transferred to the β-sheet crystalline regions;
4. Ultimate rupture as H-bonds break in the crystalline regions, which triggers the sliding of β-sheet strands (stick–slip mechanism).

Moreover, the transition between and relative moduli (stiffness) of these regimes depend on the secondary structure content. For example, for molecules with high

turn ratio and low β-sheet content, we observe an initial stiff regime, followed by a softer regime, followed by a very stiff regime leading to failure. On the other hand, systems with very high β-sheet content show a monotonically stiffening force-extension response. This suggests that the characteristic yielding behavior at the molecular level of the hierarchy of silk is controlled by the ratio of turn to β-sheet structures, where a higher turn ratio leads to the emergence of this phenomenon. This is an alternative means of achieving high initial stiffness in comparison with β-sheet content alone, which exhibits high initial stiffness as well, but provides much less extensibility. Moreover, wider secondary structure distribution exhibits a larger deviation in the initial end-to-end length, and increasing the turn content and inter-chain hydrogen bonding increases the initial stiffness and extensibility of the assembly, thereby improving the toughness as well. The failure strengths are of the same magnitude, regardless of structure content. The force-extension curves of molecular silk also show minor deviations from the inextensible chain models commonly used for polymer materials (*e.g.*, WLC models). For example, the initial stiffness at low forces until yield, due to the rearrangement and rupture of H-bonds in the amorphous domains.

As the properties of silk can vary across evolutionary lineages by over 100 % (Agnarsson et al. 2010; Swanson et al. 2009; Vollrath and Selden 2007), any quantitative parameterization (*e.g.*, critical stress and strains) are bound to a particular species. To deduce general relationships, a representative model, while limited in terms of specificity to a particular species, is used to reflect the characteristic nonlinear stress–strain behaviour of silk found in a web. From a reductionist perspective, the material behavior of silk is achieved through the combination of distinct secondary structure units in silk protein, where the interplay of the *two* distinct constituent domains characterizes the nanoscale deformation mechanisms of the emerging nanocomposite structure. Here, we can effectively "divide and conquer", with mechanical characterization of each domain independently. The benefit of such a procedure – essentially deconstructing silk into two distinct "building blocks" – is that each component can then be manipulated and potentially designed separately. Moreover, we can associate the composite behavior with the governing mechanism(s). The simplest approach to such a model is consideration of each phase as a multi-linear spring (Nova et al. 2010). The equation for two springs can be formulated as:

$$k_{silk}\left(\Delta_{silk}\right) = \left[\frac{1}{k_{crystal}\left(\Delta_{crystal}\right)} + \frac{1}{k_{amorph}\left(\Delta_{amorph}\right)}\right]^{-1} \tag{12.1}$$

Where $k_{crystal}$ represents the nonlinear stiffness of the crystalline phase, k_{amorph} the semi-amorphous domain, and the deformation of each represented by Δ (note that for a given load, $\Delta_{crystal} \neq \Delta_{amorph}$, but $\Delta_{silk} = \Delta_{crystal} + \Delta_{amorph}$). This simple "two-phase" structure of silk, with associated nonlinear force-displacement behaviors, is sufficient to describe the four regimes characteristic of dragline silk. More importantly, the separation of phases can quantify the contributions and

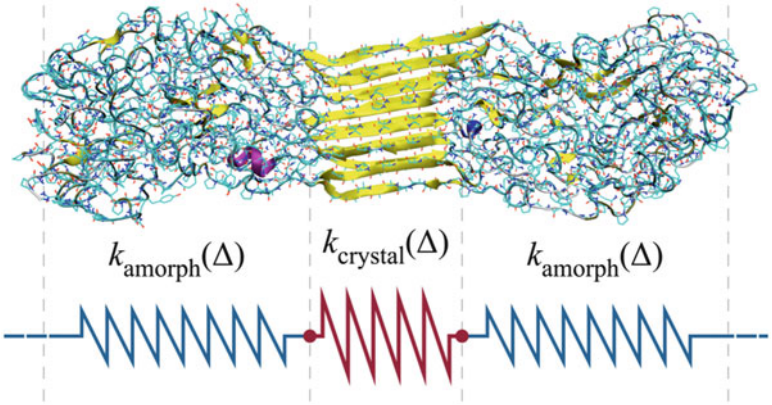

Fig. 12.4 Mechanical description through simple building blocks: silk as a simple serial spring model. The constitutive behavior of two elements (β-sheet nanocrystals and semi-amorphous domains) can be represented by simple spring relations to generate a model of silk (Eq. 12.1). Here, $k_{crystal}$ represents the nonlinear stiffness of the crystalline phase, k_{amorph} the semi-amorphous domain, and the deformation of each represented by Δ. The simple "two-phase" serial combination of these regimes (with associated nonlinear force-displacement behaviors) results in the 4-regime composite behavior depicted in Fig. 12.5, described by Eq. (12.2). Such an abstract separation of behavior allows efficient exploration of potential behaviors of silk, with parametric investigation possible through variations of crystal size, strength, "hidden length", backbone stiffness, and others (Motivated by Nova et al. 2010)

molecular mechanisms of each component – the crystalline or semi-amorphous domains – to performance metrics of silk such as strength, extensibility, and toughness (see Fig. 12.4).

Using the simple formulation above, the constitutive behavior of silk can be parameterized from the described full atomistic simulations of dragline spider silk (Keten et al. 2010; Nova et al. 2010), which accounts for the combined behavior of β-sheet nanocrystals (Keten et al. 2010) and semi-amorphous protein domains (Keten et al. 2010) that compose silk at the nanoscale (van Beek et al. 2002), typically unaccounted for in large-scale web studies (Aoyanagi and Okumura 2010; Ko and Jovicic 2004; Alam et al. 2007). A combination of multi-linear and exponential functions is used to determine the stress–strain behavior of the silk. The exponential function depicted expresses the simultaneous unfolding behavior of the amorphous regime and the transfer of load to the stiffer beta-sheet nanocrystals. The resulting function is expressed as:

$$\sigma(\varepsilon) = \begin{cases} E_1\varepsilon, & 0 \le \varepsilon < \varepsilon_y \\ \exp\left[\alpha\left(\varepsilon - \varepsilon_y\right)\right] + \beta\left(\varepsilon - \varepsilon_y\right) + C_1, & \varepsilon_y \le \varepsilon < \varepsilon_s \\ E_2\left(\varepsilon - \varepsilon_s\right) + C_2, & \varepsilon_s \le \varepsilon < \varepsilon_b \\ 0, & \varepsilon \ge \varepsilon_b \end{cases} \tag{12.2}$$

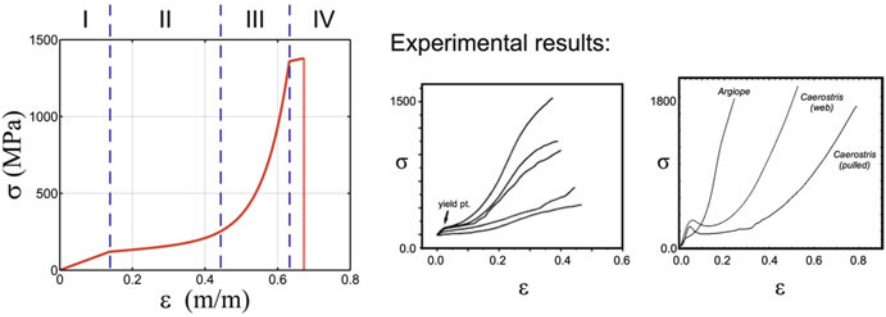

Fig. 12.5 Derived constitutive behavior parameterized from full atomistic simulations of dragline spider silk and validated against experimentally measured behaviors (*right*). Again, the behavior can be separated into four distinct regimes: (1) Initial loading in which stress is transferred *via* the poly-amorphous polypeptides, followed by a defined yield point. (2) Entropic unfolding where "hidden length" is achieved *via* sequential rupturing of 3_1-helices and β-turns. (3) Stiffening due to alignment of chains and β-sheet nanocrystals sustaining increases in applied stress. (4) Stick–slip mechanism of the β-sheet nanocrystal is triggered for a relatively small regime, and governs further deformation until ultimate rupture. While ultimately based on full atomistic molecular modeling, the derived behavior is in good agreement with the observed behavior of silk threads at the macroscale – exhibiting characteristic yield and stiffening, for example – suggesting that the molecular model can be used as a proxy to "interpret" macroscale web response. *Left*: Du et al. (2006), used with permission, copyright © 2006 Elsevier Inc.; *Right*: Agnarsson et al. (2010), copyright © 2010 used with permission under Creative Commons Attribution License

defined by four parameters (E_1, E_2, α, and β) reflecting stiffness, and three corresponding to critical strains (ε_y, ε_s, ε_b). The constants, C_1 and C_2, ensure continuity between the linear and exponential regimes. We find that the resulting stress–strain curve displays the characteristic shape observed experimentally in silk (Du et al. 2006), that is, an early yield point with associated softening, followed by a severe stiffening effect, until failure (Fig. 12.5). A key aspect of the model used here is that with such an approach, each regime of the stress–strain behavior can be directly linked to phenomena at the molecular scale. Specifically, the model illustrates four critical nonlinear behaviors found in virtually all types of silk: (1) the yield point; (2) the entropic unfolding regime where the associated H-bonded 3_1-helices and β-turns begin to rupture resulting in a high extensibility under relatively low stress; (3) severe stiffening, and; (4) ultimate rupture. To maintain *de facto* independence from empirical data, only molecular behavior is considered for model parameterization. Being said, the maximum stress level, on the order of 1–2 GPa, is in quantitative agreement with results from experimental studies (Du et al. 2006).

We note that the ultimate failure strain implemented is larger than that determined by experiment (Du et al. 2006; Ko and Jovicic 2004; Kohler and Vollrath 1995; Lin and Sobek 1998), as the nano-to-macro scaling assumption inherently admittedly lacks statistical variability and structural defects. This generally leads to enhanced strength and extensibility in comparison to physical silk systems. Furthermore,

physiologically silks undergo substantial prestretching while being spun (Du et al. 2006; Papadopoulos et al. 2009). The current atomistically derived stress–strain behavior does not incorporate the potential effect of prestretch, and we consequently expect an overestimation of the stretching capacity of the silk. Future refinements could directly include variability of structure and defects in silk and model the effect of prestretching to allow a better comparison with experimental data. In addition, the direct scaling of nanoscale behavior to macroscale behavior serves to homogenize the silk thread structure, which has been suggested to have an organized, hierarchical microstructure (Vollrath et al. 1996).

12.3 From Silk Threads to Spider Webs

The ultimate, overarching hierarchical level of silk is the spider web, exemplifying a highly organized functional geometry (Vollrath and Mohren 1985; Vollrath 2010; Aoyanagi and Okumura 2010; Ko and Jovicic 2004; Alam et al. 2007). In effect, we use the material knowledge to construct a representative structural web model as an archetype for assessing performance. Of particular interest is response to local load (*i.e.*, representing prey capture) and global load (*i.e.*, webs subject to wind). In terms of geometry, of the tremendous diversity of spider web types, the orbicular webs of the araneid orb weaving spiders are the most accessible analytically (Vollrath 1992; Aoyanagi and Okumura 2010; Zschokke and Vollrath 1995), characterized by radial threads (or "spokes") supporting an arithmetic spiral. The model architecture and geometry implemented here are borrowed from natural orb-web design (Swanson et al. 2007). The web model is then formulated based on the general material behaviour previously described, with radial and spiral threads consisting of particles connected by springs, exhibiting scaled behavior derived from mechanical characterization of the protein composite.

This modeling implementation allows for a direct relation between molecular configuration and web deformation state – *i.e.*, loading and failure of the web can be directly related to the molecular structure. We can trace a direct connection between the molecular unfolding mechanisms and the effective capacity of the web to resist load and mitigate damage through localization of failure. We note that both radial and spiral threads are modeled based on the dragline silk behavior, though in Nature these silks exhibit different material properties. This issue has been addressed in previous work (Cranford et al. 2012), where approximated spiral thread behavior, based on dragline silk, was compared to an empirically derived material model; and where both models exhibit a similar response. Finally, by intentional design, this model does not account for the intermediate fibril scale, to gain a fundamental-level understanding of deformation. We justify this choice by noting again that atomistically-derived material behavior compares well with empirical studies of silk threads (Du et al. 2006) (depicted in Fig. 12.5).

12.3.1 Defects and Flaw Tolerance

Our first analysis of web performance focuses on existing defects. As a functional structure for a spider, it is rare to see a perfectly intact spider web – *in situ* debris, loading, or changes in anchoring conditions – can easily lead to loss of silk threads (Fig. 12.6a). Yet, given the metabolic effort required by the spider for rebuilding a web, the web must still function well for prey capture in spite of minor damage (a food source is still required to produce the "repair" silk efficiently). Indeed it has been shown, using static truss analysis and linear-elastic material laws, that under tension, loading any broken thread has only a local effect and that a spider web is still capable of functioning effectively as a net for catching prey (Alam et al. 2007). Other computational studies have suggested a remarkable damage tolerance of webs (Aoyanagi and Okumura 2010) based on similar linear-elastic spring model. However, the missing piece of understanding remaining is where this damage tolerance is rooted in and specifically, how it relates to the unique molecular structure of silk. To explore the concept of flaw-tolerance – the capacity of the web to function *in lieu* of structural damage – the ability of the web to tolerate defects was assessed by systematically eliminating web sections while applying a localized load to the web.

It was demonstrated that removal of single elements and even large portions of threads away from the load have very little impact on the web behavior and failure mechanism of the web as a whole; the overall force-displacement behavior of the web remains marginally affected (Fig. 12.6b). From a fly's perspective, it is difficult to tell if it was captured by an intact or degraded web. Moreover, a detailed analysis of the failure mechanisms indicates that web failure is highly localized, occurring immediately surrounding the loaded region. Notably, localized failure occurs even if the entire web undergoes large elastic deformation. Qualitative *in situ* experiments on physical webs corroborated this computational prediction. The experimental results provide direct evidence of the localized failure of a spider web, in direct agreement with the computational predictions.

The unique localization of damage in a spider web can be directly explicated through the behavior of silk protein constituents on the molecular level, which express the underlying mechanism behind this remarkable structural property: prior to failure the vast majority of radial threads in the web exhibit relatively small stress states, equivalent to the yielding regimes of the amorphous regions. Large stress and thus deformation is highly localized on the silk thread where load is applied. Notably, unlike in the rest of the web, at the thread where load is applied the amorphous regions are almost fully unfolded and β-sheet nanocrystals begin to stretch at the particular segment of the thread to which force is applied. Since the nanocrystals are not continuous, once they locally fail, the thread ruptures (and the fly escapes!).

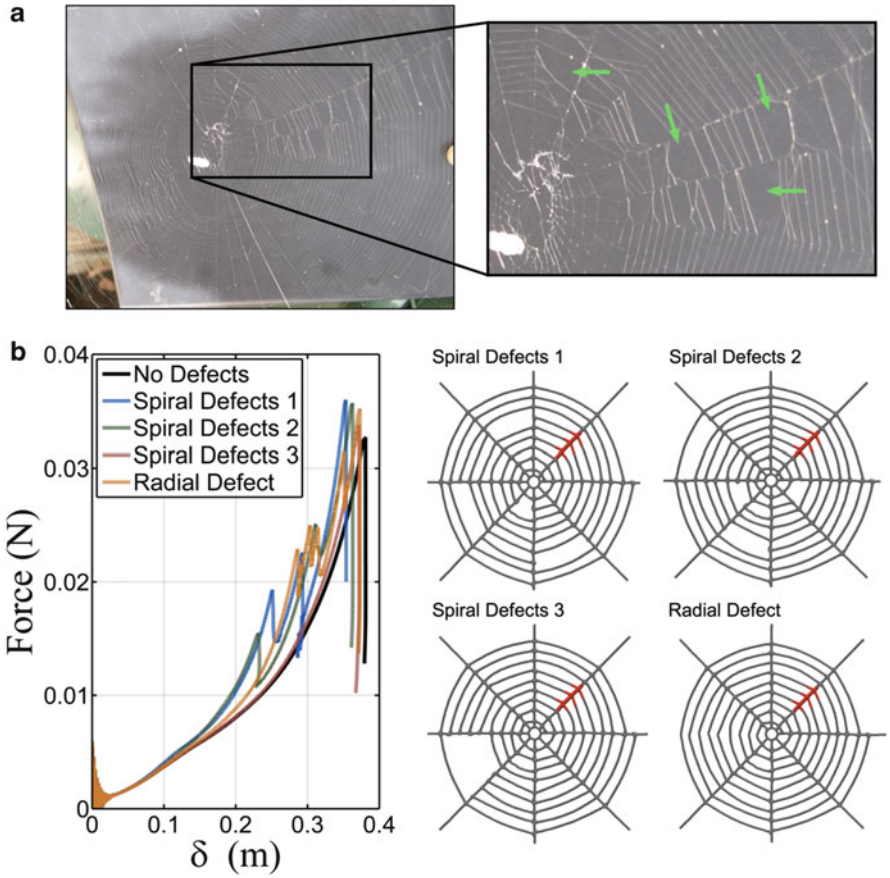

Fig. 12.6 Evidence of defects and flaw tolerance. (**a**) Photographs of *in situ* orb web of European garden spider as discovered, containing many defects and geometric irregularities. Missing spiral segments are common, supporting the radial threads (dragline) provide structural support. (**b**) Computational studies of defective web (loaded region depicted in *red*). Case studies presented include randomized missing spiral segments (Spiral Defects 1 and 2), a concentration of missing spiral segments (Spiral Defects 3) and a missing radial thread (Radial Defect). The overall force-displacement behavior of the web remains marginally affected by defects, with irregularities induced by defects within close proximity to the load (Adapted from Cranford et al. 2012)

12.3.2 Constitutive Behavior Comparison

Computational and experimental evidence clearly indicate that localized failure is a universal characteristic of spider webs, which we can directly relate to the molecular structure. However, still unresolved is whether such behavior is unique to silk material or rather the unique web-architecture, thereby motivating the scrutiny of other ideal material behaviors. Remarkably, evidence suggests that, in

opposition to popular thinking, the notable strength and extensibility of spider silk are not the primary factors, but rather it is the constitutive material behavior – the unique relation between an applied load and extension – that is essential to the function of a web. Testing this hypothesis, a systematic comparison with drastically different material behaviors that differ distinctly from that found in natural silk was undertaken (Fig. 12.7), using three mechanical models for the thread behavior that reflect extreme cases of nonlinear material behavior: (i), the atomistically-derived nonlinear behavior of natural silk; (ii), an ideal linear-elastic behavior, and (iii), an elastic-perfectly-plastic behavior that involves plastic yield. For all three models, the failure stress and strain are constant, and thus any advantage of the material will only rely on the differences in the material behavior rather than ultimate strength and extensibility.

The analysis of the deformation mechanisms for the three cases indicated that in the case of natural silk, while all radial elements contribute partially to the resistance of the applied load, the sudden yield and softening of the material introduces a weaker load path, and the loaded radial continues to resist the majority of force. The subsequent stiffening behavior facilitates the transfer of load to a localized, single radial element until ultimate failure occurs. For the linear-elastic behavior, while the loaded radial thread is still subject to the bulk of the load, the auxiliary radials and specifically those closest to the loaded thread bear a higher proportion of the ultimate load at the point of failure, thereby revealing a greater delocalization of damage in the web. For the elastic-perfectly-plastic model, the plastic yielding of a radial leads to an even further load distribution throughout the radials of the entire web structure, resulting in a greatly increased damage zone that extends through almost one quarter of the web. Interestingly, this increased contribution of the auxiliary radials results in a higher maximum strength depicted in the web-level force-displacement plots, while simultaneously resulting in less ultimate displacement. This suggests that both linear-elastic and elastic–plastic models result in a more catastrophic, brittle-like failure with significantly increased damage zones. For the natural silk behavior, the radial threads effectively become the sole sacrificial elements, while the majority of the web-structure remains intact and functional. The small decrease in ultimate strength in natural silk is superseded by greatly enhanced structural robustness, allowing a spider to repair rather than rebuild, should a failure event occur. This suggests that more deformable, yet weaker, web construction results in an overall more efficient web in its natural environment. This is highly perplexing to a practicing engineer! Unlike engineered structures, which are typically designed for ultimate loads, the forces a web could be naturally subject to are great relative to the web strength, *e.g.* a falling branch, a passing animal or a gust of wind. With the impossible task of designing for ultimate load negated, deformation capacity and structural robustness are likely more critical for the species' survival, properties that the tacit behavior of dragline silk provide as a construction material for webs!

The most important conclusion from this multi-material investigation is that silk, in its natural function as a structural element of a web, is not a "super-material" due to its strength, but rather due to its distinct nonlinear softening and stiffening

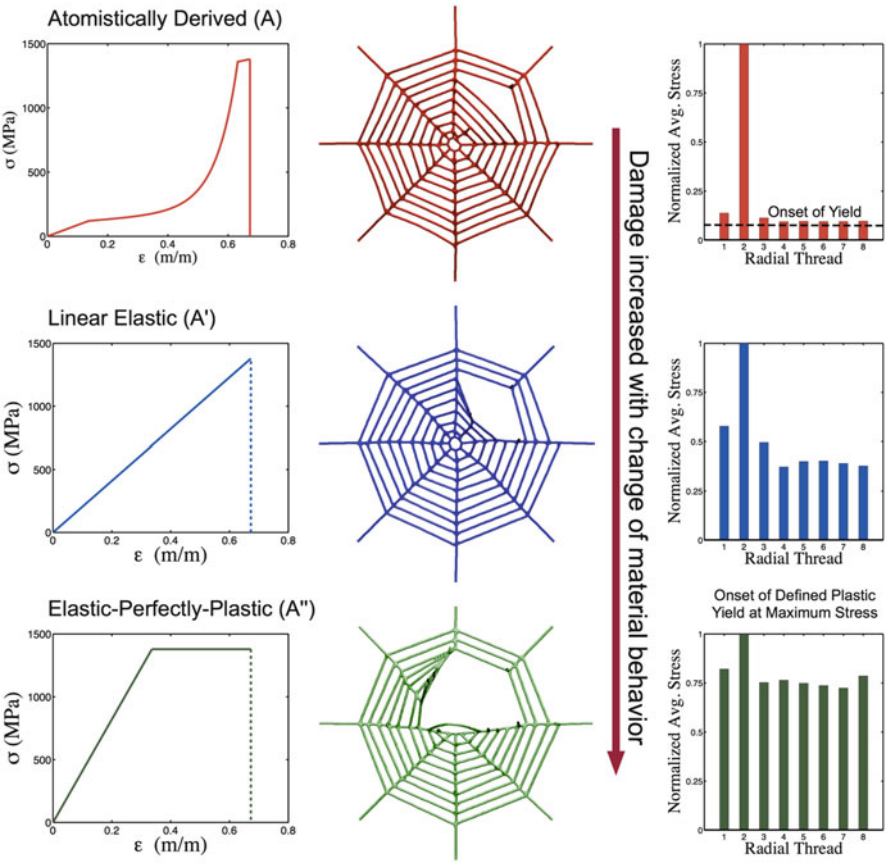

Fig. 12.7 The merging of material and structural performance. Comparison of web failure with a change in material behavior for atomistically derived silk behavior, ideal linear elastic behavior, and ideal elastic–plastic behavior, all which have the same ultimate strain and ultimate stress, demonstrates the advantage of silk as a material. Comparison of failure between the three models (*center panels*) confirms localized stresses and minimized damage for the natural hyperelastic stiffening silk behavior. A basis for macroscale-to-molecular interpretation lies in the analysis of the average stress of individual silk threads (*bar plots*; *right*) to determine distributions of molecular deformation states in the web. When load is applied locally to a radial thread, other radial threads not subject to applied force reach a maximum stress corresponding to the onset of yielding. The elastic-perfectly-plastic behavior (nonlinear softening) leads to an almost homogeneous distribution of stress in the web radials. Silk threads act as sacrificial structural elements – the easily fail to protect the web from incurring significant damage (Adapted from Cranford et al. 2012 and Cranford and Buehler 2012)

behavior, reflecting a particular type of nonlinear material behavior. Notably, while studies of other biomaterials (*e.g.*, of bone or nacre) have shown that their great mechanical robustness is due to the formation of rather large plastic regions (which facilitate the redistribution of mechanical energy over vast material volumes (Gao

et al. 2003; Kamat et al. 2000; Buehler and Yung 2009; Tang et al. 2003; Fratzl 2008; Espinosa et al. 2009)) our findings show that the opposite is true at the scale of spider webs. Here, extreme localization of failure is the key to explain its overall mechanical performance. This result suggests a change in the paradigm of material design as a function of scale, where traditional perspectives of superior mechanical properties can be drastically enhanced by integrating the design of a material's nonlinear material behavior that is defined by a particular molecular makeup. Specifically, the material behavior itself can be more significant to a system than specific quantities such as ultimate strength upon failure. It is counterintuitive that the inherent softening of silk – often viewed as a material weakness – vastly enhances the structural robustness of a web.

The hyperelastic stiffening of silk appears to enhance web robustness under localized loading – but it does not explain why silk typically has a relatively large initial stiffness (due to the H-bonding of the amorphous regime). For that, we turn to distributed or global loading – *e.g.*, the case of wind.

12.3.3 Stability Under Global Loading

To understand the response of a web under global loading (*i.e.*, loading across all radial and spiral threads), the web models were subject to a homogeneously distributed wind load, with effective wind speeds up to 70 m/s (a threshold at which all thread anchorages fail). Again, three material models – model silk, linear elastic, and elastic-perfectly-plastic – were investigated for comparison (Fig. 12.8).

To model the effect of wind, the effect of drag on the silk threads is applied, borrowing the procedure for applying wind drag on cable bridges (Poulin and Larsen 2007). The static drag wind load on a stay cable can be written as:

$$F_{\mathrm{d}} = \frac{1}{2}\rho_{\mathrm{air}} U^2 C_D A \tag{12.3}$$

where ρ_{air} is the air density, U the mean wind speed, A the reference area of the silk thread ($A = r_0 \times$ diameter) and C_{D} the drag coefficient in the along-wind direction (conservatively taken as 1.2, typical value for structural wires and cables (Poulin and Larsen 2007)).

The web is subject to constant loading with equivalent wind speeds ranging from 0.5 to 70 m/s (reaching up to strong hurricane level winds), which the maximum deflection was measured (relative to the anchoring points), applied for approximately 100 s. For wind speeds $<$10 m/s there is little difference between all material behaviours, and deflections are $<$12 % of the total span. This is because the structural rigidity of the web is attributed to the initial stiffness of the dragline silk prior to yield. Under higher wind loads, however, the softening behaviour of dragline silk at moderate deformation results in significant web deflection, greater than in the cases of linear elastic and the elastic-perfectly-plastic behaviour. Regardless of

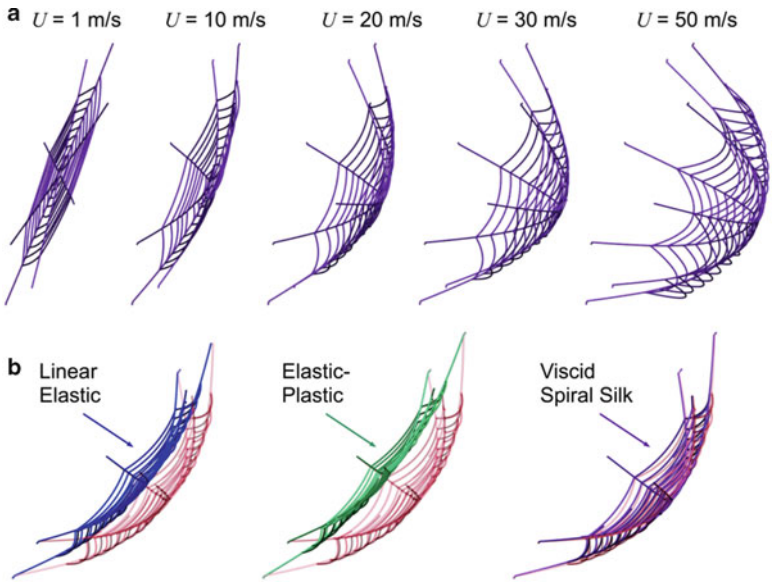

Fig. 12.8 Webs response subject to distributed or global (wind) loading. (**a**) Snapshots of computational model web response under increasing wind speeds. Yield is apparent as deformation increases rapidly with increase in wind load (drag). (**b**) Visualizations of web deflection for varying material models under a constant wind speed of $U = 20$ m/s, including linear elastic, elastic-perfectly-plastic, and a viscid spiral thread model (more compliant than dragline silk). In all cases the atomistically derived model is used as basis of comparison. As shown, the "engineered" materials (linear elastic and elastic-perfectly-plastic) are more rigid, with little deformation at such wind loads (Adapted from Cranford et al. 2012)

material behaviour, the web structure can withstand hurricane level wind speeds (speeds of approximately 40 m/s are defined as Category 1 hurricanes) prior to failure. Similarly, all webs fail at wind speeds exceeding approximately 60 m/s (Category 4 hurricane level). It is noted that while the wind loading applied is ideal (symmetric, homogenous, and constant), the results indicate a large resistance to wind-type loading due to the combined small mass and cross-section of the web silk elements. Moreover, the system-level deflection curves are indicative of the implemented constitutive material behaviour – the response of the radial threads (which ultimately transfer the wind load to the anchoring points) dominates the behaviour of the web itself. While the spiral threads undergo increased deflection and capture more of the wind load due to their larger exposed length, they are effectively pinned to the much stiffer dragline radial threads, which limit web deflection. That being said, the global wind load investigation led to three main findings:

1. The nonlinear stiffening behaviour is disadvantageous to web performance subject to large distributed forces. Yielding occurs in multiple threads simultaneously, leading to large web deflections under "extreme" wind loading.

2. The initial stiffness of dragline silk provides structural integrity under functional, or operational, conditions (expected typical wind speeds). Web rigidity is maintained and deflection is comparable to the traditional engineered material behaviours (linear elastic and elastic-perfectly-plastic).
3. The greater extensibility of viscid silk (versus dragline silk) only nominally affects the system-level response, as the load is transferred to the anchoring points *via* the radial threads, which are much stiffer.

These findings suggest that whereas the nonlinear stiffening response of dragline silk is crucial to reduce damage of localized loading, it is disadvantageous to global (*i.e.*, distributed) loading scenarios. Yielding caused by the high wind loading results in web displacements that could cause large areas of the sticky catching-spiral to impact surrounding environment (such as vegetation), which would result in the large-scale destruction of a web. However, under moderate wind loading, the linear regime of the dragline silk dominates behaviour, and silk performs as well as the other material behaviours. The wind load cases illustrate that the initial stiffness of the dragline provide structural integrity under such "global" loading conditions. Moreover, the spider itself requires a certain "nominal structural stiffness" to navigate the web. If this loading becomes "extreme" there is no benefit, and the silk yields. Presumably, what is considered "extreme" or "normal" environmental is dependent on the locale of the spider, and our approach can systematically link variation in the mechanical properties between silks of different species to such environmental loading conditions. For the silk model here, the yield occurs at wind speeds exceeding 5 m/s, defining a reasonable regime of operational wind speeds.

So, if we wish to design a spider web, we should use a material with initial stiffness (for stability under working conditions), yield, and then hyperelastic stiffening (when subject to large localized loads). But how much stiffening is required? To answer this question, we required a more theoretical description of the failure of such webs, and we turn to the field of fracture mechanics.

12.3.4 Damage Minimization and Fracture Mechanics

To investigate the failure of the webs, we implement a modified formulation of fracture mechanics, accounting for the discrete nature of webs, called Quantized Fracture Mechanics (QFM). QFM is relevant to the fracture of small discrete mesh-like structures such as nanotubes, nanowires, and nanoplates and was developed to handle the discreteness of matter at the atomistic scale, yet equally applicable to discrete mesh-like structures such as the spider web. Here we apply QFM to model the results of the simulations and experimental studies that show that nonlinear material behaviour of natural silk begets large web robustness against localized attacks and generalize the observations for different materials and structures. Classical Linear Elastic Fracture Mechanics (LEFM) cannot reach this goal since

it is based on linear elasticity and on the assumption of a continuum, which is not valid in a discrete structure such as a web.

We proceed to present a simple theoretical argument to generalize the observations for different materials and structures, while incorporating the nonlinear hyperelastic response of silk in general. We consider the simplest structure that will give us general insights, an elastic plate with a crack of length $2a$ subjected at its centre to a pair of applied forces per unit width, F. The stress-intensity factor at the crack tips is:

$$K_I = \frac{F}{\sqrt{\pi a}} \tag{12.4}$$

According to LEFM the crack will start to propagate when the stress-intensity factor equals the material fracture toughness, K_{IC}, thus for an initial crack length shorter than:

$$a_C = \frac{1}{\pi}\left(\frac{F}{K_{IC}}\right)^2 \tag{12.5}$$

(here quasi-static crack propagation is stable, different from the Griffith case). According to QFM and in contrast to classical theory the crack will propagate not when $K_I = K_{IC}$, but when

$$K_I^* = \sqrt{\frac{1}{q}\int_a^{a+q} K_I^2(a)\mathrm{d}a} = K_{IC},$$

and thus when the applied force per unit width is:

$$F = \frac{K_{IC}\sqrt{\pi q}}{\sqrt{\ln\left(1+\frac{q}{a_C}\right)}}. \tag{12.6}$$

In Eqs. (12.5) and (12.6) q is the fracture *quantum*, representing the characteristic size of the structure; and here q is the size of the web's mesh spacing and a measure of the discreteness of the system. Comparing Eqs. (12.5) and (12.6) we note that the prediction of QFM is equivalent to that of LEFM if an equivalent toughness $K_{IC}^{(q)}$ is assumed in the classical LEFM approach:

$$K_{IC}^{(q)} = \frac{K_{IC}}{\sqrt{\frac{a_C}{q}\ln\left(1+\frac{q}{a_C}\right)}} \cong K_{IC}\left(1+\frac{q}{4a_C}\right). \tag{12.7}$$

Equation (12.7) shows that in the case of a localized targeted load (in contrast to the less critical case of distributed loading) the discrete nature of the structure

helps in increasing its robustness since $K_{IC}^{(q)} \propto q$. This implies that the critical crack length a_C is reduced due to the discrete nature of the structure, as suggested by the asymptotic limit given by Eq. (12.6):

$$a_C \cong \frac{1}{\pi}\left(\frac{F}{K_{IC}}\right)^2 - \frac{q}{2}. \tag{12.8}$$

In order to generalize the concept to different constitutive laws that define the unique relationship of how stress σ versus strain ε behaves, we consider a general nonlinear stress–strain law in the form of a power law $\sigma \sim \varepsilon^{\kappa}$. Here $\kappa < 1$ denotes elastic–plastic behaviour (nonlinear softening), $\kappa = 1$ linear elasticity, and $\kappa > 1$ represents a nonlinear stiffening material. The limiting cases are $\kappa = 0$ (perfectly plastic material) and $\kappa = \infty$ (perfectly nonlinear stiffening material). The power of the stress-singularity at the crack tip will be modified from the classical value of 1/2 to (Rice and Rosengre 1968):

$$\alpha = \frac{\kappa}{\kappa + 1}, \tag{12.9}$$

and we define α as the nonlinearity parameter (linear elastic case when $\alpha = 1/2$, stiffening when $\alpha \to 1$ and softening when $\alpha \to 0$). Thus, the singularity changes similarly to what occurs at the tip of a re-entrant corner, edge cut, or crack (Carpinteri and Pugno 2005). Based on QFM theory (Pugno et al. 2008) we predict the critical force per unit width $F^{(\alpha)}$ for a nonlinear material described by the exponent α, as a function of the critical force per unit length for linear elasticity $\left(F^{(1/2)}\right)$ and perfect plasticity $\left(F^{(1)}\right)$:

$$\frac{F^{(\alpha)}}{F^{(1)}} = \left(\frac{F^{(1/2)}}{F^{(1)}}\right)^{2\alpha}. \tag{12.10}$$

It is apparent that Eq. (12.10) is general and not related to the web structure under study. It shows that the critical force in a structure changes as a function of the material constitutive law, in relation to the critical force for the linear elastic case $\left(F^{(1/2)}\right)$. Defining $\left(F^{(1)}\right) =: f$ as the breaking force per unit width of a single structural element (a spider silk thread), Eq. (12.6) becomes:

$$F = f\left(\frac{K_{IC}}{f}\right)^{2\alpha}\left(\frac{\pi q}{\ln\left(1\frac{q}{a_C}\right)}\right)^{\alpha}. \tag{12.11}$$

In the limit of $q \to 0$, Eq. (12.11) defines the equivalent fracture toughness due to the nonlinearity of the stress–strain law:

$$K_{IC}^{(\alpha)} = K_{IC}^{2\alpha}\left(\frac{f}{\sqrt{\pi a}}\right)^{1-2\alpha}. \tag{12.12}$$

Since by definition $F > f$ during dynamic failure, Eq. (12.12) suggests that $K_{IC}^{(\alpha)}$ increases with α, and accordingly the emergence of nonlinear stiffening as $\alpha \to 1$ presents a toughening mechanism. Moreover, Eq. (12.8) becomes:

$$a_C = \frac{1}{\pi}\left(\frac{F}{f}\right)^{\frac{1}{\alpha}}\left(\frac{f}{K_{IC}}\right)^2. \tag{12.13}$$

More generally, mixing discreteness and nonlinearity gives an equivalent structural fracture toughness of:

$$K_{IC}^{(\alpha,q)} = \frac{f}{\sqrt{\pi a_C}}\left(\frac{K_{IC}}{f}\right)^{2\alpha}\left(\frac{\pi q}{\ln\left(1+\frac{q}{a_C}\right)}\right)^{\alpha} \tag{12.14}$$

from where an interaction between discreteness and the nonlinearity of the stress–strain law can be deduced. Asymptotically, the critical crack length becomes:

$$a_C = \frac{1}{\pi}\left(\frac{F}{f}\right)^{\frac{1}{\alpha}}\left(\frac{f}{K_{IC}}\right)^2 - \frac{q}{2}. \tag{12.15}$$

The QFM predictions of Eqs. (12.14) and (12.15) suggest strategies in the impact mitigating design of spider web inspired structures. Most importantly, both the discreteness (measured by q) and nonlinear stiffening (measure by α) represent toughening mechanisms against failure under localized loading. Equation (12.15) shows that the damaged zone after failure has a characteristic size that diverges as the exponent α is decreased (*i.e.*, $\alpha \to 0$ so that the material approaches a softening stress–strain behaviour). In order to take the discreteness of the structure into account we introduce Eq. (12.5) into Eq. (12.10) and find for the ratio of damaged material:

$$\varphi(\alpha) = \left(\frac{a_C^{(\alpha)}}{a_C^{(1)}}\right)^2 \tag{12.16}$$

Since by definition $a_C^{(1)}$ represents the overall size of the entire structure, $\varphi(\alpha)$ represents the damaged area fraction of the structure after failure. Further, by expanding Eq. (12.16) we arrive at

$$\left(\frac{a_C^{(\alpha)}}{a_C^{(1)}}\right)^2 = \left(\frac{a_C^{(1/2)}}{a_C^{(1)}}\right)^{4\alpha} = \left(\varphi^{(1/2)}\right)^{2\alpha} = S^{2\alpha} = \varphi(\alpha). \tag{12.17}$$

Herein $S = \varphi^{(1/2)}$ is a system-dependent constant that represents the ratio of damaged material associated with linear elastic behaviour. Considering a heterogeneous structure composed by n different materials (such as dragline and viscid silks as found in natural orb webs), with volumetric ratios v_i $\left(\sum_{i=1}^{n} v_i = 1\right)$ and described by n different constitutive law exponents α_i, we expect ratios of damaged materials in the phases i equal to:

$$\varphi^{(i,\alpha_i)} = \left(\varphi^{(i,1/2)}\right)^{2\alpha_i} = \left(S^{(i)}\right)^{2\alpha_i} \tag{12.18}$$

Equation (12.18) explicitly shows that the larger stiffening effect, the more localized the damaged zone. Note that $\varphi^{(1/2)}$ represents the structural response for the classical case of linear elasticity and thus represents a structural parameter (S). From the given arguments, S is a structural property, dependent on the specific material properties (such as fracture toughness, σ_c), system geometry (*i.e.* crack width, a or element length), and applied loading conditions, representing the relative damage associated with linear elastic behaviour (*i.e.* from the original LEFM assumption). Likewise, expressed in terms of all structural components:

$$\varphi = \sum_{i=1}^{n} \varphi^{(i,\alpha_i)} v_i . \tag{12.19}$$

The "structural robustness" Ω is defined as the fraction of surviving material in the structure after failure has occurred:

$$\Omega = 1 - \varphi = 1 - S^{2\alpha}. \tag{12.20}$$

Consequently, the relative size of the damage zone is a function of the material constitutive law. The result of Eq. (12.20) is depicted in Fig. 12.9 for a single material structure. We recognize that fixing all other variables, the larger the material nonlinearity parameter α the larger the structural robustness. Therefore, generally and independent from the specific material behaviour of silk, a more pronounced the material stiffening with strain, the larger the structural robustness as failure is increasingly localized, thus resulting in failure of a minimal number of elements in a discrete mesh-like structure (Pugno et al. 2008).

Defining web damage as percentage of failed (broken) threads, we observe a range from 2.5 % for the natural silk behaviour to 15 % for the elastic-perfectly-plastic model, a relative increase of 600 % (Fig. 12.7, centre panel). For our simulation observations, the number of broken elements (defined as failure of a thread between successive spiral-radial connections after loading) for the derived (hyperelastic) silk behavior, linear elastic, and elastic-perfectly-plastic constitutive models respectively. Using the linear-elastic results as a reference, we can back-calculate the theoretical hyperelastic or nonlinearity parameters for our specific web geometry. We calculate the structural parameter $S \approx 0.06$ (for such a value, there is significant deviation of structural robustness from hyper-elastic to plastic

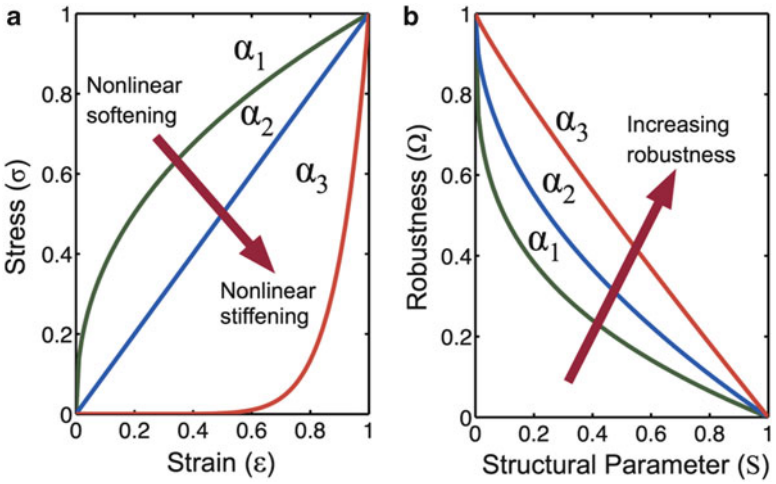

Fig. 12.9 Effects of stress–strain behaviour on structural robustness *via* Quantized Fracture Mechanics (QFM). (**a**) Plots of considered stress–strain curves (material behaviour) demonstrating the transition from softening to stiffening behaviours by the nonlinear parameter α ($\alpha_1 = 0.3$, $\alpha_2 = 0.5$, $\alpha_3 = 0.9$). (**b**) Structural robustness, Ω, defined as the undamaged fraction of the structure, versus system-dependent constant *S*. The parameter S is system dependent, reflecting a range of material properties (such as fracture toughness), system geometry (*i.e.* crack width or element length), and applied loading conditions. Universally, the robustness increases with an increase in α ($\alpha_1 < \alpha_2 < \alpha_3$); *e.g.* larger nonlinear stiffening results in larger structural robustness, and thus, less damage (Adapted from Cranford et al. 2012)

behavior). The comparison between the simulations and QFM predictions show good agreement.

We find that based on this theory, akin to the finding our simulations and experiments in webs, the key to reach minimal structural damage is that the material undergoes a severe increase in stiffness under applied stress. This phenomenon is duly exemplified in spider webs, where the nonlinear stiffening behaviour as $\alpha > 1$ is essential for localized damage; and a loaded thread becomes a sacrificial element while the majority of the web remains intact. Again, given the presumed metabolic effort required by the spider for rebuilding an entire web, localized failure is preferential as it does not compromise its structural integrity**,** and hence continues to function for prey capture in spite of damage. Figure 12.9 shows varied stress–strain behaviors treated with QFM theory, revealing that the size of the damaged zone in the proximity to a defect increases for materials that tend to feature a softening behaviour as realized in the elastic–plastic model (Rice and Rosengre 1968). Conversely, the realization of a stiffening material behaviour results in a decrease of the damage zone. This directly shows that the introduction of nonlinear behaviour dictates the relative size of the damage zone (Pugno et al. 2008). As demonstrated in the theoretical analysis, our findings generally hold for other

materials (including nanostructures) in which the material's stress–strain behaviour dictates functionality beyond limit parameters, such as the ultimate strength.

In spider webs we have demonstrated that the cooperative action of a stiffening structural member (the radial silk thread under load) and yielding (or softening) of ancillary members result in a localization of elastic resistance. Concurrently, adjacent radials reveal partly unfolded amorphous regions, or a partially stiffened state – immediately after failure, load is redistributed between these two adjacent threads, keeping the rest of the web intact and functional. Indeed, sections of the web removed from loading undergo limited deformation and strain. This property of the web architecture and silk's unique nonlinear behavior combine to form a structure designed to tolerate damage by inducing localized failure of redundant structural elements. In sum, for spider webs, when small loads are applied to the web, the entire web structure deforms and contributes to mechanical resistance. However, once loading exceeds the critical load necessary for molecular unfolding, localization of deformation occurs, and thus very few web elements fail at the ultimate breaking point.

These results show that independent from the specific material behaviour of silk, a more pronounced the material stiffening with strain, the larger the structural robustness as failure is increasingly localized, thus resulting in failure of a minimal number of elements in a discrete mesh-like structure (Pugno et al. 2008). As shown, this phenomenon is duly exemplified in webs, where the combined yielding-stiffening nonlinear material behaviour provides an ideal medium for localized damage and thus structural robustness. This behavior can be deemed a structural liability if local failure (such as cracking) can lead to catastrophic collapse, irreparable damage, mechanical instabilities, or degradation of system function. The existence of a web-like mesh structure, however, is critical as the failure of few elements does not lead to the catastrophic breakdown of the material as demonstrated in Fig. 12.6. For spider webs such localized failure is preferred, as structural elements effectively dissipate energy from the applied load and can be sacrificed (and replaced) without comprising the structural integrity and functionality of the entire system. This suggests the use as a practical design principle where the same "localized damage" can be expressed in synthetic systems by implementing a constitutive behavior inspired by silk, or, more generally, a deliberate increase in nonlinear material behavior to realize a significant stiffening as strain increases, as shown in Fig. 12.9. Thus, the simple relation of structural failure mechanisms to nonlinear material behaviour revealed here can be easily applied in the design of structural components in which minimal damage is desired. For example it motivates the use of sacrificial elements introduced in buildings and bridges for seismic and terrorist protection, or generally for the design of highly robust structures and armours.

A general finding of this study is that superior performance does not need to rely on the strength of elementary building blocks, but rather, on the integration of material and structure. These findings were the first to demonstrate that the superior functionality of spider silk to the overall performance of webs is based on the unique yielding-stiffening behavior rather than the relatively high values of

ultimate strength and strain. Silk's inherent material nonlinearity is responsible for its advantage over linear-elastic or elastic–plastic materials such as steel or concrete, making it the preferred building material for robust web structures. This work explains the fundamental issue of how the functionality of biological construction materials – in this case, spider silk – extends beyond traditional concepts of strength and strain by utilizing specific deformation mechanisms as loading is increased. The approach presented can be adopted by scientists working on a diverse range of interdisciplinary fields related to polymers, biological materials, and other synthetic systems, where the inclusion of nonlinear material in the design process behavior can impede structural loss, minimize damage, localize failure, and increase system robustness and integrity. Such a holistic and multi-scale optimization of function through molecular structure and mechanical behavior can lead to the development of fundamental discoveries.

The web model, like any computational model exploited by mechanicians, is constrained to its prescribed boundary conditions, or the ideal anchorage of the radial threads. Structural engineering principles dictate that any loading – be it local or global – is ultimately transferred to the supports or structural foundation. One structural feature of the web that remains poorly understood is the attachment disc – a network of silk fibers that mechanically anchors a web to its environment. One would expect that the web attachments or anchorages are very robust in Nature, yet very little is known about these structures, and they too are deserving of investigation.

12.4 "Universal" Attachments

The discussed web model in the previous section assumed ideal fixity – that is, the extended radial threads were secured to assure web failure occurred within the interior of the web structure and not at the attachment (or anchorage) sites. While we have suggested that webs themselves are robust and flaw tolerant, how precise must a spider construct the structures that attach a web to its environment? Uncertainty and variation in environmental conditions suggest a need for robust and adaptable anchorages – a "universal" attachment system – yet webs illustrate reproducible and deliberate geometric construction. Hence, we proceed to utilize the same silk material model to examine the mechanism of itegrated optimization of material and structure *via* a detailed analysis of a silk attachment disc (Blasingame et al. 2009), one possible structure used to anchor webs to their physical surroundings (cementing dragline silks to a variety of solid supports such as wood, concrete, or other surfaces during web construction). We exploit dragline silk as our basis material, which has been observed to fuse with attachment disc silk, providing a secure anchor point to assist prey capture and predator evasion (Blasingame et al. 2009; Sahni et al. 2012), often referred to as a "safety line" for the spider (Gosline et al. 1999).

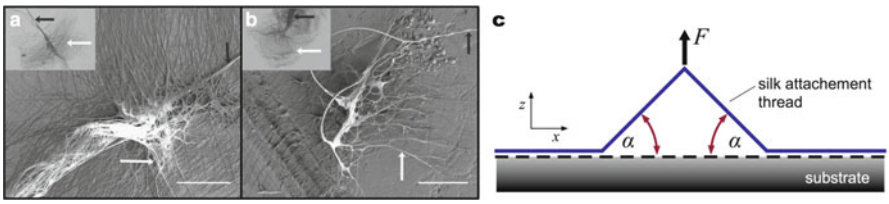

Fig. 12.10 Web anchorage and "universal" attachments. (**a–b**) Attachment disc morphologies. Figure shows SEM images of scaffolding discs (**a**) and gumfoot discs (**b**) spun by the cobweb-weaving spider *A. tepidariorum*. Insets show optical microscope images of the respective discs. The *black arrows* point towards dragline silk in (**a**) and its inset, while the *white arrows* point towards pyriform silk fibres, arranged in a 'staple-pin' architecture, attaching the dragline silk to the surface. *Black arrows* point towards gumfoot thread (MA silk covered with aggregate glue) in (**b**) and its inset, while the *white arrows* point towards pyriform fibres, arranged in a dendritic architecture, attaching the gumfoot thread to the surface. Scale bars in both the figures are 100 μm. From Shani et al. (2012), used with permission, copyright © 2012, Macmillan Publishers Limited. (**c**) Model silk attachment for theoretical/computational investigation defined as a colarchic, symmetric, two-branched adhesive anchorage (simple anchorage). The force F is applied perpendicularly to the substrate (Adapted from Pugno et al. 2013)

Experimental observations suggest that one possible attachment disc arrangement adheres to a substrate through multiple symmetrically branched structures composed of sub-micrometer scale silk fibers (Fig. 12.10a, b). Again, we note that the evolutionary diversity of spiders have resulted in a vast array of material properties and behaviours (Agnarsson et al. 2010; Swanson et al. 2007; Vollrath and Selden 2007), web structures (Vollrath and Selden 2007; Blackledge et al. 2009; Craig 1987), and, not surprisingly, associated means of attachment (Sahni et al. 2012; Geurts et al. 2010). For example, a recent study has elucidated both "staple-pin" like attachments for structural anchorage, and branching "dendritic" structures for prey-capture (Sahni et al. 2012). That being said, both architectures are similar at the fiber/substrate interface – that is, significant lengths of silk splayed across the substrate from common superstructure (*i.e.*, dragline thread). For example, in "staple-pin" morphologies, the threads are ordered in a linear fashion, whereas "dendritic" structures exhibit radial branching. Irrespective of superstructure, the splayed configurations can be idealized at the interface of thread and substrate, where adhesion/anchorage ultimately occurs, which we use as an archetype structure for mechanical analysis. Again, our goal is not to exactly replicate the silk attachment, but rather learn the physics underwriting Nature's success.

Such splayed attachment discs display remarkable adhesive properties and hold great potential to guide the design of bio-inspired and biomimetic anchorages and adhesives (Pugno and Lepore 2008). The hierarchical arrangement of the anchorage – wherein few dragline threads are splayed into numerous contact fibers – is remarkably similar to the gecko's foot where thousands of keratinous setae, only one-tenth the diameter of a human hair, adhere to a surface (Autumn et al. 2000). The morphological convergence of hierarchical branched adhesive pads in

lizards, spiders and several insect orders, for example, indicates an advantage of this design for substrate adhesion (Varenberg et al. 2010; Arzt et al. 2003; Gao and Yao 2004; Filippov et al. 2011). Due to the physiological role, the problem of branched adhesion has been investigated previously from the perspective of attachment and detachment cycles and related biomechanical functions (Pugno and Lepore 2008; Autumn et al. 2000). Moreover, early functional explanations of such adhesive organs focused on the performance on rough substrates, where flexible branched fibers can make more intimate contact, control detachment and increase adhesion (Gao and Yao 2004; Federle 2006). In contrast, the attachment disc of a spider web is a *passive* structure, wherein secure attachment (optimal adhesion) is the primary goal, subsidiary to ease of detachment. Unlike the gecko's foot, for example, the attachment must provide a permanent anchorage of a spider's web upon construction. As such, analysis and computational experiments focus on peeling strength and toughness to investigate the material and structural synergy of the anchorage. Currently, little is known about the intricate, branched structure of the attachment disc (Fig. 12.10a, b) or the mechanical properties of the silk that compose it (Lewis 2006; Vollrath and Knight 2001; Sahni et al. 2012; Geurts et al. 2010).

Again, we look to Nature and biological systems (nay, models), to serve a technical application of practical purpose – a need to develop theory rather than replicate performance. We hence propose to explore the attachment disk with a general elastic theory of a multiple-branched adhesive anchorage and optimize it from both a material and structural perspective. We proceed to describe a theoretical model to explore the adaptation of the strength of attachment of such an anchorage, validated by complementary simulations to demonstrate a novel mechanism of synergetic material and structural optimization, such that the maximum anchorage strength can be achieved regardless of the initial anchor placement or material type.

12.4.1 Theory of Multiple Peeling

We consider our archetype structural model depicted in Fig. 12.10c that shows a simple anchorage to reflect the geometry identified in SEM imaging. Note that this can be considered the simplest substructure of either "dendritic" or "staple-pin" morphologies, capturing the thread/substrate interaction. A simple anchorage is defined as a colarchic, two-branched, symmetrical, adhesive anchorage. It is an adhesive anchorage because it allows a force, F, to be transmitted to a solid substrate through adhesive forces at the material interface (*e.g.*, no penetration of material entanglement), symmetrical because the angles, α, on both side are equal, and it is colarchic because it has no hierarchy. The model represents the most basic geometry of anchorages that engage adhesive forces at the structure-substrate interface. It is used here as the starting point for a systematic analysis based on the theory of multiple peeling (Pugno 2011).

In an earlier work (Pugno 2011) it was proposed an elastic theory model of the simple anchorage with adhesive forces at the branch-substrate interface, and found that the critical delamination force is:

$$F_{\mathrm{d}} = 2Y A_{\mathrm{c}} \sin\alpha \varepsilon_{\mathrm{d}} \tag{12.21}$$

where Y is the elastic modulus, A_{c} is the branch cross-sectional area and ε_{d} is the critical level of strain at which a branch will delaminate. Balancing the critical delamination force, strain, adhesion energy, and contact angle, yields:

$$\varepsilon_{\mathrm{d}} = \left[\cos(\alpha) - 1 + \sqrt{(1-\cos(\alpha))^2 + \lambda}\right], \tag{12.22}$$

where ε_{d} is the critical level of strain to initiate delamination, and α the contact angle (Pugno 2011). We introduce a nondimensional parameter, λ, representing the competition between adhesion energy per unit length, γ, and elasticity ($\lambda = 4\gamma/(Y A_{\mathrm{c}})$; where Y is the elastic modulus and A_{c} is the cross-sectional area of a branch). Hence, the contact angle α is a parameter that can change the critical delamination force through strain (ε_{d} decreases as $\alpha \to 90°$). A single adhered branch with a free end can be delaminated with lower force with induced variation in geometry. Indeed, it is has been shown that the unique macroscopic orientation and preloading of a gecko seta can successfully increase attachment force, while suitably orientated setae can reduce the forces necessary to peel the toe by simply detaching above a critical angle with the substrate (Autumn et al. 2000; Tian et al. 2006) – a geometrically induced attachment/detachment trigger. Again, this mechanism is facilitated by the unidirectionality and cooperativity of the gecko's seta (Autumn et al. 2000; Tian et al. 2006) – a feature not present in the two-branched anchorage. Silk anchorages, however, are multi-branched in varied directions (in the case of dendritic branching), or symmetric (in the case of staple-pin morphologies), captured by the simple multi-branch model. Variation in attachment angle can not be easily achieved without initiating delamination – increasing the contact angle on one adhered branch subsequently decreases the angle of the opposite. Therefore, for stable anchorage of spider webs, directionally opposed pairs minimize the loss of adhesion due to geometric changes in the angle.

There exists an optimal angle, $\alpha_{\max}$, that maximizes the delamination force and is dependent on λ. Substituting Eq. (12.22) into (12.21) for ε_{d}, finding where the derivative of the structural delamination force with respect to α is equal to zero corresponding to a force maximum:

$$\frac{\mathrm{d}F_{\mathrm{d}}}{\mathrm{d}\alpha} = 2Y A_{\mathrm{c}} \left[\cos\alpha \left(\cos\alpha - 1 + \sqrt{(1-\cos\alpha)^2 + \lambda}\right) + \sin\alpha \left(-\sin\alpha + \frac{(1-\cos\alpha)\sin\alpha}{\sqrt{(1-\cos\alpha)^2 + \lambda}}\right)\right] = 0 \tag{12.23}$$

from which we derive:

$$\cos(\alpha_{\max}) = \frac{1}{\cos(\alpha_{\max}) + \sqrt{(1-\cos(\alpha_{\max}))^2 + \lambda}} = \frac{1}{1+\varepsilon_d}. \tag{12.24}$$

Simply put, the force required for delamination is geometrically restricted by the peeling angle, $\alpha_{\max}$, assuming homogeneous anchorage along the length of contact. We note that $\alpha_{\max} \to 90°$ as the material becomes increasingly compliant ($\varepsilon_d \to \infty$), while $\alpha_{\max} \to 0°$ with an increase in stiffness ($\varepsilon_d \to 0$). This result also implies that the force required for delamination is geometrically restricted by the contact angle, $\alpha_{\max}$. A fixed peeling angle, α, enables the variation of delamination force from a negligible to a very significant value. More importantly, we find that an optimal contact angle, $\alpha_{\max}$, maximizes the delamination force and depends on λ.

12.4.2 Synergetic Optimization of Structure and Material

The design of the anchorage can be optimized by stipulating that material failure and delamination occur at the same load, similar to the principle of optimal design of laminate composites wherein all layers in the composite are designed to fail simultaneously – no material strength is left unused. This implies comparable probabilistic failures of the attachment discs and silk fibers in agreement with observations in preliminary experiments conducted on spider webs. The strictly economic design principles that have been noted in the architecture of spider webs (Lewis 2006; Gosline et al. 1986; Opell 1998) are necessary for a creature that internally produces all of its own building material. That the spider web uses a remarkably tiny volume of material to cover a relatively broad area is an evident example of this type of economy, but volume of material may not be the only measure of cost – as indicated, the great strength of major ampullate silk fibers, such as dragline silk, is due to nanoscale β-crystals (Keten et al. 2010; Keten and Buehler 2010a; Termonia 1994; Nova et al. 2010). The production of these super-strong crystals have an extra metabolic cost to the spider (Craig et al. 1999; Blamires et al. 2012; Bratzel and Buehler 2012) – one which would be purely wasteful in a condition where an incongruency between adhesive and strength failure leaves the strength capacity unused.

Setting the delamination strain to equal the material's ultimate strain (ε_p), we pose the condition of simultaneous failure where $F_p^{opt} = F_d$ and as a result $\varepsilon_p^{opt} = \varepsilon_d$. Equations (12.22) and (12.24) can therefore be rewritten to relate the optimal material strain $\left(\varepsilon_p^{opt}\right)$ to the optimal angle $(\alpha_{\max})$:

$$\varepsilon_p^{opt} = \frac{1}{\cos(\alpha_{\max})} - 1 \tag{12.25}$$

Equation (12.25) shows that material behaviour elicits a particular structural optimization, and a direct relation between λ and ε_p can be found from Eq. (12.22):

$$\lambda^{opt} = \left(\varepsilon_p^{opt}\right)^2 + 2\varepsilon_p^{opt}\left(1 - \frac{1}{1+\varepsilon_p^{opt}}\right). \tag{12.26}$$

Equations (12.25) and (12.26) describe simultaneous structural (α^{opt}, λ^{opt}) and material (ε^{opt}) optimizations.

Among the types of silk found in spider webs, it has been noted that dragline and flagelliform silks absorb more energy prior to failure than almost any commonly used material (Lewis 2006). If we define energetic capacity as the elastic energy until failure as T (toughness modulus), we can further relate the optimal energetic capacity, strength, and strain. The optimal strength of the simple anchorage (the subscript "1" denotes properties which refer to this structure) with simultaneous material failure and delamination is:

$$F_1^{opt} = 8\gamma \frac{\sqrt{\left(\varepsilon_p^{opt}\right)^2 + 2\varepsilon_p^{opt}}}{\left(\varepsilon_p^{opt}\right)^2 + 3\varepsilon_p^{opt}} \tag{12.27}$$

The energetic capacity in the linear elastic domain of the simple structure which we are considering is:

$$\frac{T_1^{opt}}{L} = 2\left(\frac{1}{2}\sigma_p^{opt}\varepsilon_p^{opt}A_c\right) = 4\gamma\frac{1+\varepsilon_p^{opt}}{3+\varepsilon_p^{opt}} \tag{12.28}$$

We denominate the energetic capacity T in reference to the material property "toughness" although here we discuss a structural property; L is the branch length. The energetic capacity increases asymptotically with yield strain (ε_p^{opt}) up to a value of 4γ.

Manipulation of Eqs. (12.27) and (12.28) to eliminate γ yields:

$$\frac{T_1^{opt}}{L} = 4\gamma\frac{1+\varepsilon_p^{opt}}{3+\varepsilon_p^{opt}} = F_1^{opt}\frac{\left(\varepsilon_p^{opt}\right)^2 + \varepsilon_p^{opt}}{2\sqrt{\left(\varepsilon_p^{opt}\right)^2 + 2\varepsilon_p^{opt}}} \tag{12.29a}$$

From which it is apparent that:

$$T_1^{opt} \to 4\gamma L \text{ as } \varepsilon_p^{opt} \to \infty \tag{12.29b}$$

and

$$F_1^{opt} \to 0 \text{ as } \varepsilon_p^{opt} \to \infty \tag{12.29c}$$

We find that $T^{\text{opt}} \sim \varepsilon_{\text{p}}^{\text{opt}}$, whereas $F^{\text{opt}} \sim 1/\varepsilon_{\text{p}}^{\text{opt}}$. This relation indicates a second benefit to compliance (*i.e.*, increased detachment strain), whereby the energy capacitance increases to maximize the adhesion (*e.g.*, $T^{\text{opt}} \to 4\gamma L$ as $\varepsilon_{\text{p}}^{\text{opt}} \to \infty$) under simultaneous material failure and delamination. Note that this does not hold for simple detachment – as previously stated, the relative stiffness of the gecko's toe allows for easy detachment by inducing the critical angle required for delamination – it is presumed the gecko does not want a toe to fracture simultaneously!

The definition of toughness illustrates a trade-off where high values of ε_{p} lead to a relatively high energetic capacity and a relatively low force capacity, while for low values of ε_{p} the opposite is true. Polymeric adhesives (such as tapes) are preferably soft such that able to deform sufficiently for intimate contact over a relatively large surface area and maximize adhesion (Gay and Leibler 1999). Indeed, when two materials are brought into contact, their surface roughness is crucial to determine the quality of contact and hence the intensity of adhesion (similar to why household tape sticks better by pushing it into a contact with a surface). The same benefit can be associated with the silk attachment disc, flexible and extensible threads can easily adapt to the topography of rough substrates and achieve a more intimate contact, and thus compliant silk is beneficial.

12.4.3 Hierarchical Branching: Smaller Is Stronger

Inspired by the vast number of tiny anchorages of which the attachment disc is composed (see Fig. 12.10a, b), we pose the question: is there an advantage in a greater number of attachments? A similar scaling effect was exploited earlier by introducing the principle of contact splitting (Arzt et al. 2003), whereby dividing a structure into finer subcontacts increases adhesion (Pugno 2011). If adhesive forces scale linearly with the dimensions of the contact, as they do here, the adhesive strength scales with the peeling edge length and not with the area (Varenberg et al. 2010; Arzt et al. 2003). One inherent assumption of this argument is that the pull-off stress is distributed uniformly over all the contacts, and delamination occurs simultaneously.

Extending this concept, as an alternative to the simple structure with two branches, we consider an analogous structure with $2N$ symmetrical branches with equivalent cross-section. The structural force and energy capacity can be rewritten in terms of the constant volume, $V = 2Na_cL$. For a thread of constant volume and length both energy capacity, T, and strength, F, increase with a decrease in cross-sectional area, a_{c}. The total cross-sectional area is conserved between the cone and simple structures, that is $A_{\text{c}} = Na_{\text{c}}$, where a_{c} is the cross-sectional area of an individual branch, and N the total number of branches. The total strength, F_N, of the structure will be:

$$F_N = 2Y\,(Na_c)\sin\alpha\varepsilon_p \tag{12.30}$$

Given that the critical delamination in our model (Eq. (12.21)) is equal to the value found by Kendall for single-branch peeling (Kendall 1975), we find our extension of the theory to higher values of N to be reasonable (Pugno 2011). Consequently, the nondimensional parameter λ is increased by a factor of $\sqrt{N}$:

$$\lambda_N = \sqrt{N}\lambda_1 \tag{12.31a}$$

and as a result the strength and the energetic capacity (if L is maintained constant) of the cone structure are increased by a factor of $\sqrt{N}$ with respect to the simple structure:

$$F_N = \sqrt{N}F_1 \tag{12.31b}$$

$$T_N = \sqrt{N}T_1 \tag{12.31c}$$

Finally we note that if conservation of material volume V is imposed between the cone and the simple anchorage (where $V = 2A_cL = 2Na_cL$). Substitution results in:

$$F_N = \frac{4\gamma}{a_c}\frac{\sqrt{\varepsilon_p^2 + 2\varepsilon_p}}{\varepsilon_p^2 + 3\varepsilon_p}\frac{V}{L} \tag{12.32a}$$

and

$$T_N = \frac{2\gamma}{a_c}\frac{1+\varepsilon_p}{3+\varepsilon_p}V \tag{12.32b}$$

where a_c is the cross-sectional area of a individual branch, and N the total number of branches ($A_c = Na_c$), and the volume, $V = A_cL$.

If we consider a film-like cross-sectional area, where typically $a_c = hw$, (h = height above the adhesion interface; w = contact width) we see, along with decreasing w, that the force and toughness modulus can be increased with a decreasing height of the thread or branch, h – *i.e.*, only the cross-sectional area is required to be decreased. As a result, given a peeling edge of constant width, a decrease thread cross-sectional area, without changing the contact interface, results in increased performance, similar to the effect observed in contact splitting. This can be justified through the nondimensional parameter λ, representing the balance of elastic and adhesion, which can be altered through variation of a_c, regardless of contact width w. Hence the performance of the anchorage can be optimized by having a cross-section as small as possible, whether this means using 2 or N branches, with stronger adhesion resulting from numerous fibers, supported by experimental observations (Sahni et al. 2012). A minimization of cross-sectional

area per contact thread may indicate why such anchorages are composed of a multitude of discrete contacts, rather than a continuous disc that would maximize potential adhesion area.

12.4.4 Computational Validation of Attachments

While the exact mechanical behavior of the silk composing attachment disks is unknown, it does not eliminate the possibility to explore the behavior of the attachment disc using a series of computational experiments. While unnecessary to model the exact behavior of silk constituting the attachment disc, we again wish to accurately capture the generic silk-like behavior and assess the mechanisms of detachment. Thus, for the current investigation, as a simplification, we implement the general model for dragline silk previously discussed.

First, a two-branched anchorage with varying initial angle ($\alpha_0 = 15°$, 30°, 45°, 60°, and 75°) is modeled, subject to an increasing vertical force. Upon loading, the attachment angle and applied force is tracked (Fig. 12.11). Initially there is deformation without delamination; and the angle increases. This initial change in geometry is facilitated by the inherent yielding and softening of the silk, and there is a large change in angle at a marginal applied force. Once the detachment process reaches a certain angle it maintains that angle by delaminating and deforming upwards in equal measure. Moreover, we observe that the angle evolves towards an asymptotic value which is the same regardless of the initial angle used. This means that the two-branched adhesive anchorage, laid down with an arbitrary initial angle, modifies itself with pulling towards an "intrinsic" structural angle. This asymptotic angle, α_∞, coincides with the critical angle in delamination, α_{max}, as described by Eq. (12.24). We note that it varies with the value of the adhesion parameter, γ_L, which is an input in our model. We can subsequently calculate the value of λ, where λ is used to find the theoretical values of the optimal angle, α_{max}, through Eq. (12.24). Excellent agreement was found between the asymptotic angles seen in the simulations and the theoretical critical delamination angle calculated.

To further demonstrate that the optimization occurs irrespective of the nonlinear behavior of silk, a general constitutive material law was introduced, such that strain at delamination is variable (through parameterization of stiffness and ultimate strain, but constant strength). Again, upon load, there is deformation without delamination inducing an angle increase, regardless of the model. Detachment is initiated at different angles (and, equivalently, forces), followed by convergence to an asymptotic angle, which varies as a function of extensibility. Simply put, for the same required delamination force, more compliant silk reaches a higher delamination strain, and thus a higher peeling angle. We further note that the optimal angle, α_{max}, is not reached for a general hyperelastic model. Indeed, upon delamination, the detached silk subject to load has little intrinsic stiffness, and the subsequent strain results in deviation from the optimal angle – the upward pulling of the thread can only increase the local peeling angle. This effect is amplified for

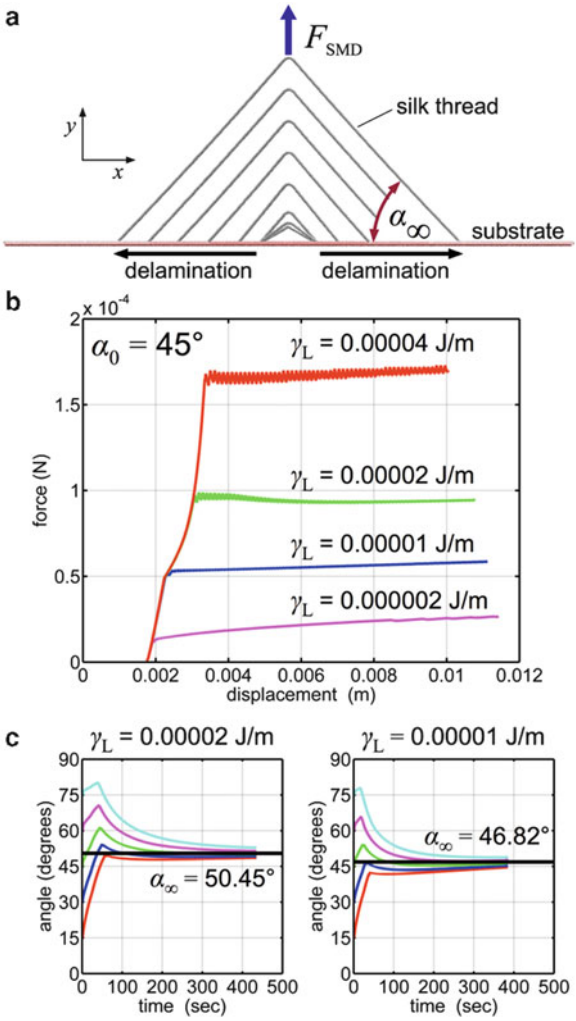

Fig. 12.11 Summary of peeling simulations. (**a**) Silk model for two-branched peeling simulations in with prescribed adhesion energy, γ_L, and attachment angle, α_0. Snapshots depict evolution of attachment angle under load with $\alpha_0 = 30°$ and $\gamma_L = 2 \times 10^{-5}$ J/m (50 s. increments). (**b**) Applied force versus attachment structure displacement, for $\alpha_0 = 45°$ and γ_L from 0.2×10^{-5} J/m to 4.0×10^{-5} J/m. (**c**) Measured angle versus times for peeling simulations with silk model for varying substrate interaction values $\gamma_L = 0.00002$ J/m and $\gamma_L = 0.00001$ J/m; initial attachment angles, α_0, of 15°, 30°, 45°, 60°, and 75°; regardless of initial attachment angle, the detachment angle approaches an asymptotic value, α_∞, upon delamination (50.45° and 46.82° for 0.00002 J/m and 0.00001 J/m respectively) (From Pugno et al. 2013)

stiff silks, where the difference in stiffness changes dramatically with strain. For the previous nonlinear model, the effect was negated by the initial silk stiffness prior to yield – the detaching segments are intrinsically stiffer than the free thread. In both cases, for optimal performance, extensibility of the attachment silk is an asset. The simulation of different materials verifies the validity of Eq. (12.25) as the relation between optimal delamination strain and angle, and thus applicable considering the real, currently unknown, material behavior of the attached silk anchorage. We further conclude that self-optimization cannot be reached for stiffer silks, as the dynamic peeling process cannot converge to the ideal angle.

The simulations reveal an interesting property of "self-optimization" – under load the anchorage automatically approaches the optimal configuration, by either increasing or decreasing the attachment angle. Notably, this behavior is facilitated by the intrinsic extensibility of the silk, allowing the freedom to reconfigure angles of attachment with little applied load, followed by increase in stiffness after the optimal angle is attained under stress. For the purely hyperelastic cases (no yield), attaining the optimal delamination angle was hindered by the stiffness of the silk, yet each material case was "self-optimizing". For similar silk anchorages, it has been experimentally shown that differences in pull-off forces can be attributed to differences in the size (thread diameter), chemistry (intrinsic adhesion strength) and the peeling angles (structure) of the attached threads to the substrate (Sahni et al. 2012). Extensibility of threads facilitates an internal optimization of peeling angle, thus negating the need for geometric control during construction. Although the current model is simplified compared to the complex structure of real attachment discs, the concept of "self-optimization" of adhesive anchorages provides a possible explanation for how 10,000 connections might be able to conform to function in a precise optimal configuration.

12.4.5 Detachment Under Wind Loading

To further asses the anchorage, we require a potential loading case to serve as a proxy for our simulated force and systematic load variation. Common loading scenarios in a web's natural environment are forces caused by wind, and web anchorages should adequately transfer any anticipated wind loads without detachment. Again, for a given wind speed, U, we calculate the effective drag force on a web per anchorage, F_{wind}. We assume symmetric resistance of the force, wherein each supporting radial assumes an equal fraction of the load. From these simplifying assumptions, we relate wind speed (U) to applied anchorage force (F_{wind}). The structure is then subject to a constant force allowing a conformational change until equilibrium is reached. There are three possible outcomes: (1), adhesion energy is sufficient to resist the applied force, and the structure equilibrates to a finite displacement; (2), adhesion energy is inadequate, and delamination occurs; (3), adhesion energy is sufficient to prevent delamination, but ultimate stress (fracture) is reached in the anchor. The wind speed is systematically increased until

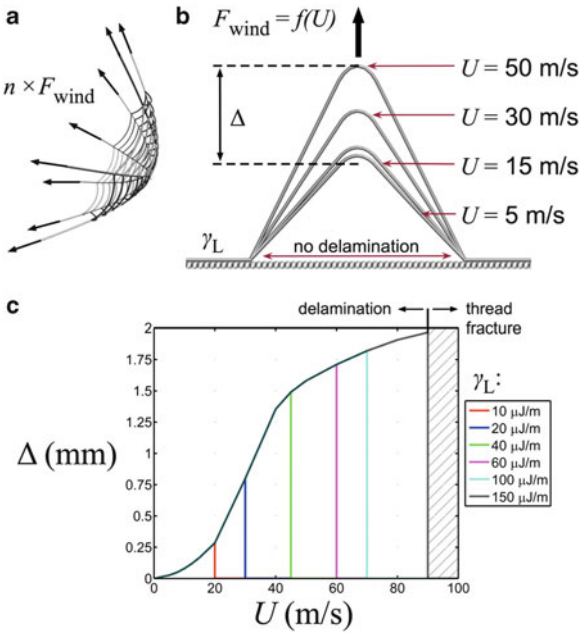

Fig. 12.12 Summary of wind load simulations. (**a**) Schematic of equivalent anchorage forces derived by constant drag force resisted by an idealized model web. (**b**) Equivalent force (F_{wind}) is applied to the model as a function of wind speed, U, and total displacement, Δ, of the anchorage is measured upon equilibration. Snapshots depict an adhesion energy of $\gamma_L = 60$ μJ/m. (**c**) Plot of wind speed versus anchorage displacement with variation in adhesion energy ($\gamma_L = 10$–150 μJ/m). At small adhesion energies, delamination occurs at relatively small wind speed. While increasing adhesion energy and thread strength can prevent delamination further, ultimate failure (fracture) of the thread will occur when the adhesion energy is on the order of 150 μJ/m (From Pugno et al. 2013)

failure by delamination occurs. Once delamination occurs, the adhesion energy is incrementally increased and the anchorage subject to further increases in applied force. This process is repeated until fracture of the threads is the failure mode (Fig. 12.12).

The mode of failure is investigated for adhesion energies ranging from $\gamma_L = 10$ μJ/m to 150 μJ/m. At small adhesion energies, delamination occurs at relatively small wind speed (delamination for winds in exceeding 20 m/s for $\gamma = 10$ μJ/m, for example). The deformation response is reflective of the constitutive stress–strain relationship for the model silk (*e.g.*, yielding and subsequent hyperelastic stiffening occurring at wind speeds >10 m/s). The simplified assumptions (such as number of anchoring radial threads, the total length of silk in a web, and the number of adhesive branches per radial thread) limit a more exact prediction of adhesion energy, but provide a realistic range subject to experimental validation and a means to systematically vary the applied load. A more refined prediction of adhesion strength is unsubstantiated, considering

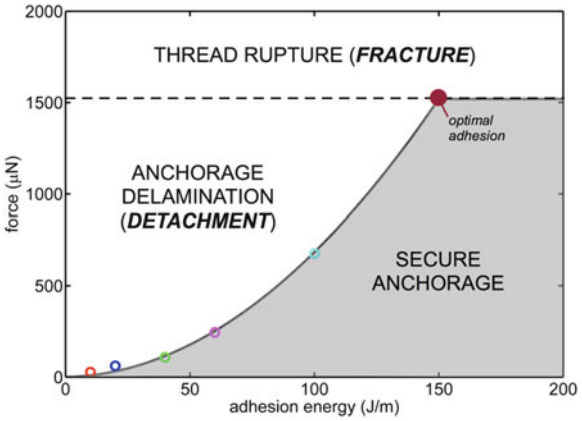

Fig. 12.13 Anchorage failure mode phase diagram. Variation of wind (Fig. 12.12) provides a means to systematically vary anchorage load. For other loadings in general (such as prey capture), a simple phase diagram can be mapped, indicating regimes of secure anchorage, delamination/detachment, and thread rupture/fracture. The plotted points ($\gamma_L = 10$, 20, 40, 60, 100, 150 μJ/m) are the results from Fig. 12.12c. For the presumed thread strength (1,400 MPa) the optimal adhesion energy is on the order of 150 μJ/m, resulting in simultaneous anchorage delamination and thread fracture (Adapted from Pugno et al. 2013)

the approximated constitutive law and the idealized fiber-substrate interaction. Variation in substrate and environment anchoring conditions (such as material chemistry, surface roughness, temperature, humidity, etc.) prohibit any single specific adhesion energy. Such uncertainties support the self-optimizing design of a two-branched anchorage system.

It behooves us to note we do not make any claims of biological importance of such wind loading. Indeed, our drag force calculation is depended on the idealized orb-web model (Cranford et al. 2012; Tarakanova and Buehler 2012b), and directly proportional to the presumed length of the capture silk spiral (providing drag resistance) and number of radials threads (*i.e.*, the number of anchors distributing the load). The aim is to illustrate the change in failure mechanism (*i.e.*, detachment/delamination *v*. thread rupture) as a function of load in order to optimize the material strength and/or adhesion energy. In a similar fashion, other loading conditions (such as prey capture, spider movement, etc.) could be mapped to particular silk behaviours to delineate optimal adhesion with constitutive material response through an effective phase diagram (see Fig. 12.13). Estimation of such loads and a survey of silk behaviour is beyond our expertise and intent of the investigation.

In spite of such contingencies, the computational results indicate a range of adhesion strengths in a physically reasonable regime. While the constitutive relation employed is representative of major ampullate dragline silk, the attainable ultimate stress and strain is within the same order of magnitude as other, empirically characterized silks (Agnarsson et al. 2010). Increasing adhesion energy can prevent delamination further, limited by ultimate failure (fracture) of the anchor threads, occurring when the adhesion energy is on the order of 150 μJ/m (subject to the

limiting strength of the model silk, ≈1,400 MPa). Thus, this value ultimate sets the upper bound for predicted adhesion energy, based simply on the ultimate stress of the dragline threads. A value of adhesion energy on the order of 150 μJ/m is optimal uniformly strong silk anchorages (simultaneous delamination and rupture). In addition, for the current silk anchorage model, the yield occurs at wind speeds exceeding 10 m/s, defining a reasonable regime of operational wind speeds, below which structural integrity of a web anchorage is maintained. Interspecies variation of this yield point (Agnarsson et al. 2010) may predict the wind conditions a web is subjected to.

Experimentally, using silk anchorages on glass, failure by fracture (*i.e.*, dragline rupture) rather than delamination was consistently observed (Sahni et al. 2012). This suggests an overcapacity of adhesion strength for the tested substrate. Indeed, even in consideration of evolutionary demands, the spider cannot be expected to optimize material usage and performance for all possible cases. With a requirement that the anchorages must be robust enough for a variety of substrates, evolution may have driven the failure mode to rely on the silk strength (produced by the spider) rather than an unknown substrate (produced by the environment).

Structurally, a balance of the delamination force (F_d) and strain (ε_d) results in an intrinsic optimal delamination (or peeling) angle (α_{max}) which maximizes the adhesion strength of the anchorage. A potential tunable variable for other biological adhesive systems (such as the gecko's seta), this maximizing angle is facilitated by the initial two-branched V-shape of the attachment disk, and symmetric yet opposing directionality of the fibers in contact with the substrate. While investigations contact splitting has elucidated the benefits of multiple adhesion threads (Arzt et al. 2003; Gao and Yao 2004; Filippov et al. 2011), and the angle of peeling has been delinated as a critical delamination parameter (Autumn et al. 2000; Tian et al. 2006), the coupling of hierachical branching, cooperative delamination, and the convergence to optimal angle is a key insight revealed by the spider's attachment disk. Moreover, from a materials perspective, the inherent extensibility of silk acts as a natural guide, allowing the structural arrangement of the anchorage to reconfigure and "find" the optimal angle under load, regardless of initial geometry, suggesting such attachments do not require precise placement by the spider *in situ*. As a result, little effort is needed to survey potential (successful) anchorage sites. It seems Spiderman's nonchalant targeting of Manhattan skyscraper ledges to adhere his web has biological evidence – the attachment will naturally optimize upon load. Indeed, rather than redesign, a spider employs an anchorage that, while not universal, can adequately perform under a range of conditions.

12.5 Conclusion

In hierarchical modeling of materials, the model allows for a convenient link between length scales, bridging scales through pinpointing assembly and deformation mechanisms. At the molecular level, the model of silk takes in as input

the sequence of residues, yielding structure, size characterization and material behavior parameters and mechanisms as output. The amino acid sequence dictates the chemistry of higher-order secondary protein structures: domains of low and high density of hydrogen bonds are achieved in simulation. Low density hydrogen bonding is present in the coiled, elastic domains while denser hydrogen bonding results in the mechanism of nanoconfinement, which directs the characteristic size and strength of crystals composing silk. The two domains establish a collaborative interaction contributing complementary function: strength and extensibility. The unique strength of the bottom-up analytic approach is, in addition to a more complete and accurate system description, the potential to link higher order structural scales to fundamental components at lowest hierarchical material levels – in effect, the seamless merging of material and structure. The material behavior of silk is played out on the scale of the web and the ability of the web to effectively resist load at the observable macroscale behavior to molecular mechanisms. One cannot understand the performance of a spider web without consideration of the silk response.

In the context of structural performance, the remarkable strength, toughness and extensibility of spider silk are not the dominating factors in achieving excellent structural performance of a web. Rather, it is the constitutive material behaviour, the distinct nonlinear softening and stiffening of dragline silk that is essential to function. Such behaviour results in the localization of damage to sacrificial threads in a web under targeted (local) loading while, due to the large initial stiffness, minimizing web deformations under moderate wind (global) loading. Each regime of the nonlinear material behaviour of silk plays a key role in defining the overall system response under variegated environmental settings.

Considering the behaviour of silk threads in the context of the overall mechanical response of spider webs, the performance of the web is intrinsically linked to properties of molecular building blocks, which are simple protein chains and dominated by weak H-bonding. The enhanced functionality of the web relies on the integration of material and structure across all scales. The relationship is intimate – other natural silk threads that form solid materials such as cocoons, and not assembled in aerial webs, typically display different mechanical responses (Shao and Vollrath 2002), as we should expect them too. Indeed, cocoon silk, resembling the elastic-perfectly-plastic behaviour would not be suitable for web construction, whereas dragline silk would be inappropriate for cocoons. The softening behaviour combined with a solid material structure rather than a discrete mesh results in greater spreading of damage that effectively enhances its fracture toughness, clearly an advantage for the protective role of cocoons. Studies of other biomaterials have also attributed mechanical robustness to the formation of large plastic regions (Gao et al. 2003; Kamat et al. 2000). The opposite is true for webs, where extreme localization of failure at sacrificial elements occurs, a behaviour enhanced by the stiffening of threads.

These findings suggest a practical engineering design principle, implementing material behaviour inspired by spider webs within structural components to impede structural loss, minimize damage, localize failure, and increase system robustness.

Unlike current practice where sacrificial elements are used solely to dissipate energy (*e.g.*, impact loading, seismic response), the realization of sacrificial elements in discrete structures as identified in spider webs avoids potentially dangerous system-level loading and mitigates structural damage. The small decrease in spider web load capacity is superseded by greatly enhanced structural robustness, allowing a spider to repair rather than rebuild, should failure occur. This marks a shift in structural design by ignoring the requirements for the magnitude of a potential load and allowing local failure to occur, a design stipulation that requires joint consideration of material behaviour and structural architecture. The functionality of biological construction materials extends beyond traditional concepts of strength and toughness and shows its advantage over linear elastic or elastic–plastic materials such as steel or concrete.

We have further demonstrated an intrinsic optimization mechanism of a spider web attachment disc – a kind of "universal" attachment – using an elastic theory model of a multiple branch peeling, validated by computational modeling and combined with an analysis of its natural structure. Hypothesizing that the attachment disk of the spider web must be designed with two functionalities – *i.e.* force capacity and energetic capacity, and with minimal material – we demonstrated optimization of the structure using an elastica theory model of a multiple branch adhesive anchorage. While similar to the hierarchical branched adhesive pads in lizards, spiders and several insects, the attachment disk employed by the spider exploits a different set of mechanistic principles. As the spider is both an evolutionary structural engineer and materials scientist, the optimization is both structural and material.

In both cases (web fracture and anchorage failure), the extreme hyperelasticity – *i.e.* elastic stiffening under large extension – benefits structural performance, in contrast to typical engineering practice (wherein large deformation is typically avoided). It appears that structural engineers and materials scientists alike can learn from the spider. We conceive that the ability to analytically describe multiple levels of hierarchical behavior from building blocks opens the opportunities for creating tunable materials, with the possibility of controlling properties at multiple scales simultaneously. Such analysis projects the possibility of new design paradigms in areas of application ranging from high performance fibers and multifunctional materials produced from artificially spun silk or derived materials (Omenetto and Kaplan 2010), to novel material platforms for tissue engineering or even structural applications in the defense or aerospace industry (Vepari and Kaplan 2007; Buehler and Yung 2009).

The first step in linking materials science and biology (*i.e.*, "biomimetic materials research") lies in *simplification* – learning from the original biological system and elucidation of the structure–function relationships in biological materials (Fratzl 2007; Aizenberg and Fratzl 2009). Here, we have attempted to understand the underlying design principles and mechanisms that determine optimized spider web/silk performance across scales, from molecule (*e.g.*, protein sequence) to structural components (*e.g.*, silk threads), to the associated functional structure (*e.g.*, webs and web anchorages). Rather than plagiarize Nature we need to move

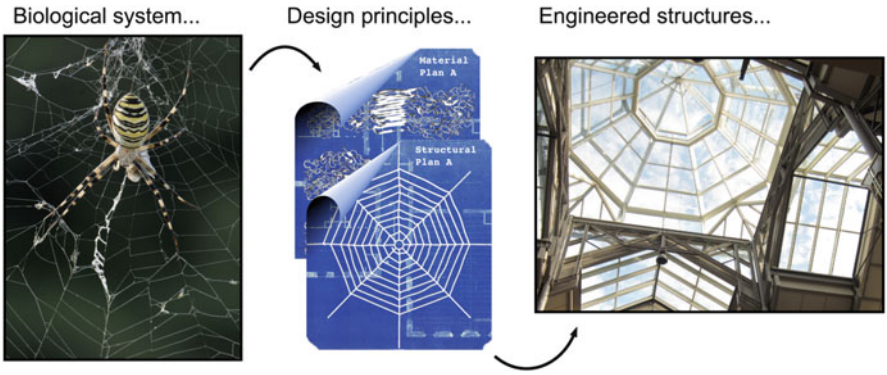

Fig. 12.14 Does bio-inspiration have a role at the macro-structural scale? While the concept of "stealing ideas from Nature" is well known, there is currently little to no impact on structural engineering. This chapter attempts to reconcile structural concepts from Nature (*e.g.*, a spider silk/web biological system) and understanding the governing phenomena (*e.g.*, failure) and design principles (*e.g.*, sacrificial elements, self-optimization) from a mechanistic perspective (*e.g.*, fracture mechanics, multiple peeling), providing the "*blueprints*" for engineered structures (Photo left by F. Tomasinelli and E. Biggi)

beyond total mimicry and enhance our understanding of the underlying physical phenomena – the functional relations that make silk a successful material – to serve as the "blueprints" for engineering design principles (Fig. 12.14). Here, we exploited quantized fracture mechanics (QFM) and the theory of multiple peeling to theoretically describe the interaction and performance of silk structures. Ultimately, the more general our understanding, the more powerful the concept, thereby increasing potential applications. We do not study silk with the hopes of building man-made webs or cocoons – we study silk to learn how to balance material structure and function from the protein sequence to a final functional system. The potential gain is the ability to make materials with similar function (and performance) but from different (and improved) building blocks.

In sum, the combined assessment of computational and experimental studies, using silk as an example, provides an understanding of the challenges currently faced within biological material analysis. Experimental methods lack the power to accurately, or definitively, describe the molecular composition of silk at atomistic levels, as a result of imaging technique limitations. Computation methods, though accessible at atomistic scales, require experimental validation on the macroscopic scale and complement experimental methods. Through prudential simplification of complex materials, scientists will be able to narrow the knowledge gap existing in the description of biological materials on computational and experimental sides, uncovering the key behaviors and parameters that govern system performance. This simplification, however, requires intimate knowledge and understanding of the entire biological system. In a seemingly paradox, we need to understand the multiscale complexity in order to successfully simplify (and therefore learn)

from the system. Only recently have technological developments enabled such advancements in the understanding of silk. We envision that such an approach to studying biological materials – including other examples such as collagen or elastin – will facilitate a better understanding of material composition, structure, and biological function across scales, and provide tools for effectively manipulating these properties to achieve superior material qualities for application in a variety of fields, from structural engineering to medicine and similar biotechnologies.

Acknowledgements NMP is supported by the European Research Council under the European Union's Seventh Framework Programme (FP7/2007-2013)/ERC Grant agreement n° 279985 (Ideas Starting Grant BIHSNAM, 2012–2016). NMP and MJB acknowledge the support from the MIT-Italy program MITOR. MJB and SWC acknowledge support from a NSF-MRSEC grant with additional support from ONR, AFOSR and ARO. SWC acknowledges additional support from Northeastern University, Department of Civil and Environmental Engineering.

References

Agnarsson I, Blackledge TA (2009) Can a spider web be too sticky? Tensile mechanics constrains the evolution of capture spiral stickiness in orb-weaving spiders. J Zool 278(2):134–140

Agnarsson I et al (2009) Supercontraction forces in spider dragline silk depend on hydration rate. Zoology 112(5):325–331

Agnarsson I, Kuntner M, Blackledge TA (2010) Bioprospecting finds the toughest biological material: extraordinary silk from a giant riverine orb spider. PLoS One 5(9):e11234

Aizenberg J, Fratzl P (2009) Biological and biomimetic materials. Adv Mater 21(4):387–388

Aizenberg J et al (2005) Skeleton of *Euplectella* sp.: structural hierarchy from the nanoscale to the macroscale. Science 309(5732):275–278

Alam MS, Jenkins CH (2005) Damage tolerance in naturally compliant structures. Int J Damage Mech 14(4):365–384

Alam MS, Wahab MA, Jenkins CH (2007) Mechanics in naturally compliant structures. Mech Mater 39(2):145–160

Aoyanagi Y, Okumura K (2010) Simple model for the mechanics of spider webs. Phys Rev Lett 104(3):038102

Arzt E, Gorb S, Spolenak R (2003) From micro to nano contacts in biological attachment devices. Proc Natl Acad Sci USA 100(19):10603–10606

Autumn K et al (2000) Adhesive force of a single gecko foot-hair. Nature 405(6787):681–685

Blackledge TA et al (2009) Reconstructing web evolution and spider diversification in the molecular era. Proc Natl Acad Sci USA 106(13):5229–5234

Blamires SJ, Wu CL, Tso IM (2012) Variation in protein intake induces variation in spider silk expression. PLoS One 7(2):e31626

Blasingame E et al (2009) Pyriform Spidroin 1, a novel member of the silk gene family that anchors dragline silk fibers in attachment discs of the black widow spider, *Latrodectus hesperus*. J Biol Chem 284(42):29097–29108

Bosia F, Buehler MJ, Pugno NM (2010) Hierarchical simulations for the design of supertough nanofibers inspired by spider silk. Phys Rev E 82(5):056103

Boutry C, Blackledge TA (2009) Biomechanical variation of silk links spinning plasticity to spider web function. Zoology 112(6):451–460

Bratzel G, Buehler MJ (2012) Molecular mechanics of silk nanostructures under varied mechanical loading. Biopolymers 97(6):408–417

Brown CP et al (2012) Rough fibrils provide a toughening mechanism in biological fibers. ACS Nano 6(3):1961–1969
Buehler MJ (2010) Tu(r)ning weakness to strength. Nano Today 5(5):379–383
Buehler MJ, Yung YC (2009) Deformation and failure of protein materials in physiologically extreme conditions and disease. Nat Mater 8(3):175–188
Carpinteri A, Pugno N (2005) Fracture instability and limit strength condition in structures with re-entrant corners. Eng Fract Mech 72(8):1254–1267
Carpinteri A, Pugno NM (2008) Super-bridges suspended over carbon nanotube cables. J Phys Condens Matter 20(47):474213
Cetinkaya M et al (2011) Silk fiber mechanics from multiscale force distribution analysis. Biophys J 100(5):1298–1305
Craig CL (1987) The ecological and evolutionary interdependence between web architecture and web silk spun by orb web weaving spiders. Biol J Linn Soc 30(2):135–162
Craig CL et al (1999) A comparison of the composition of silk proteins produced by spiders and insects. Int J Biol Macromol 24(2–3):109–118
Cranford SW, Buehler MJ (2012) Biomateriomics, 1st edn. Springer, New York
Cranford SW et al (2012) Nonlinear material behaviour of spider silk yields robust webs. Nature 482(7383):72–76
Du N et al (2006) Design of superior spider silk: from nanostructure to mechanical properties. Biophys J 91(12):4528–4535
Elices M et al (2009) Mechanical behavior of silk during the evolution of orb-web spinning spiders. Biomacromolecules 10(7):1904–1910
Elices M et al (2011) The hidden link between supercontraction and mechanical behavior of spider silks. J Mech Behav Biomed Mater 4(5):658–669
Espinosa HD et al (2009) Merger of structure and material in nacre and bone – perspectives on de novo biomimetic materials. Prog Mater Sci 54(8):1059–1100
Federle W (2006) Why are so many adhesive pads hairy? J Exp Biol 209(14):2611–2621
Feig M, Karanicolas J, Brooks CL (2004) MMTSB tool set: enhanced sampling and multiscale modeling methods for applications in structural biology. J Mol Graph Model 22:377–395
Filippov A, Popov VL, Gorb SN (2011) Shear induced adhesion: contact mechanics of biological spatula-like attachment devices. J Theor Biol 276(1):126–131
Foelix RF (1996) Biology of spiders, 2nd edn. Oxford University Press/Georg Thieme Verlag, New York/Stuttgart, 330 p
Fratzl P (2007) Biomimetic materials research: what can we really learn from nature's structural materials? J R Soc Interface 4(15):637–642
Fratzl P (2008) Collagen: structure and mechanics. Springer, New York
Fratzl P, Barth FG (2009) Biomaterial systems for mechanosensing and actuation. Nature 462(7272):442–448
Frische S, Maunsbach AB, Vollrath F (1998) Elongate cavities and skin-core structure in Nephila spider silk observed by electron microscopy. J Microsc 189:64–70
Gao HJ, Yao HM (2004) Shape insensitive optimal adhesion of nanoscale fibrillar structures. Proc Natl Acad Sci USA 101(21):7851–7856
Gao H et al (2003) Materials become insensitive to flaws at nanoscale: lessons from nature. Proc Natl Acad Sci USA 100(10):5597–5600
Gay C, Leibler L (1999) Theory of tackiness. Phys Rev Lett 82(5):936–939
Geurts P et al (2010) Synthetic spider silk fibers spun from Pyriform Spidroin 2, a glue silk protein discovered in orb-weaving spider attachment discs. Biomacromolecules 11(12):3495–3503
Giesa T et al (2011) Nanoconfinement of spider silk fibrils begets superior strength, extensibility, and toughness. Nano Lett 11(11):5038–5046
Gosline JM, Demont ME, Denny MW (1986) The structure and properties of spider silk. Endeavour 10(1):37–43
Gosline JM et al (1999) The mechanical design of spider silks: from fibroin sequence to mechanical function. J Exp Biol 202(23):3295–3303

Guinea GV et al (2003) Self-tightening of spider silk fibers induced by moisture. Polymer 44(19):5785–5788
Hansell MH (2005) Animinal architecture, 1st edn. Oxford University Press, New York
Heim M, Romer L, Scheibel T (2010) Hierarchical structures made of proteins. The complex architecture of spider webs and their constituent silk proteins. Chem Soc Rev 39(1):156–164
Holland GP et al (2008) Determining secondary structure in spider dragline silk by carbon-carbon correlation solid-state NMR spectroscopy. J Am Chem Soc 130:9871–9877
Jelinski LW (1998) Establishing the relationship between structure and molecular function in silks. Curr Opin Solid State Mater Sci 3:237–245
Jenkins JE et al (2010) Quantitative correlation between the protein primary sequences and secondary structures in spider dragline silks. Biomacromolecules 11(1):192–200
Kamat S et al (2000) Structural basis for the fracture toughness of the shell of the conch *Strombus gigas*. Nature 405(6790):1036–1040
Kendall K (1975) Thin-film peeling – elastic term. J Phys D: Appl Phys 8(13):1449–1452
Keten S, Buehler MJ (2010a) Nanostructure and molecular mechanics of spider dragline silk protein assemblies. J R Soc Interface 7(53):1709–1721
Keten S, Buehler MJ (2010b) Atomistic model of the spider silk nanostructure. Appl Phys Lett 96(15):153701
Keten S et al (2010) Nanoconfinement controls stiffness, strength and mechanical toughness of beta-sheet crystals in silk. Nat Mater 9(4):359–367
Knippers J, Speck T (2012) Design and construction principles in nature and architecture. Bioinspir Biomim 7(1):015002
Ko FK, Jovicic J (2004) Modeling of mechanical properties and structural design of spider web. Biomacromolecules 5(3):780–785
Ko KK et al (2002) Engineering properties of spider silk. Adv Fiber Plast Laminate Compos 702:17–23
Kohler T, Vollrath F (1995) Thread biomechanics in the 2 orb-weaving spiders Araneus-diadematus (Araneae, Araneidae) and Uloborus-walckenaerius (Araneae, Uloboridae). J Exp Zool 271(1):1–17
Kummerlen J et al (1996) Local structure in spider dragline silk investigated by two-dimensional spin-diffusion nuclear magnetic resonance. Macromolecules 29:2920
Lazaris A et al (2002) Spider silk fibers spun from soluble recombinant silk produced in mammalian cells. Science 295(5554):472–476
Lefevre T, Rousseau ME, Pezolet M (2007) Protein secondary structure and orientation in silk as revealed by Raman spectromicroscopy. Biophys J 92(8):2885–2895
Lewis RV (2006) Spider silk: ancient ideas for new biomaterials. Chem Rev 106(9):3762–3774
Li SFY, Mcghie AJ, Tang SL (1994) New internal structure of spider dragline silk revealed by atomic-force microscopy. Biophys J 66(4):1209–1212
Lin LH, Sobek W (1998) Structural hierarchy in spider webs and spiderweb-type system. Struct Eng 76(4):59–64
Liu Y, Shao ZZ, Vollrath F (2005) Relationships between supercontraction and mechanical properties of spider silk. Nat Mater 4(12):901–905
Ma B, Nussinov R (2002) Molecular dynamics simulations of alanine rich beta-sheet oligomers: insight into amyloid formation. Protein Sci 11(10):2335–2350
Nova A et al (2010) Molecular and nanostructural mechanisms of deformation, strength and toughness of spider silk fibrils. Nano Lett 10(7):2626–2634
O'Brien JP et al (1998) Nylons from nature: synthetic analogs to spider silk. Adv Mater 10(15):1185
Omenetto FG, Kaplan DL (2010) New opportunities for an ancient material. Science 329(5991):528–531
Opell BD (1998) Economics of spider orb-webs: the benefits of producing adhesive capture thread and of recycling silk. Funct Ecol 12(4):613–624
Opell BD, Bond JE (2001) Changes in the mechanical properties of capture threads and the evolution of modern orb-weaving spiders. Evol Ecol Res 3(5):567–581

Papadopoulos P, Solter J, Kremer F (2009) Hierarchies in the structural organization of spider silk-a quantitative model. Colloid Polym Sci 287(2):231–236
Porter D, Vollrath F (2007) Nanoscale toughness of spider silk. Nano Today 2(3):6
Porter D, Vollrath F (2009) Silk as a biomimetic ideal for structural polymers. Adv Mater 21(4):487–492
Porter D, Vollrath F, Shao Z (2005) Predicting the mechanical properties of spider silk as a model nanostructured polymer. Eur Phys J E Soft Matter 16(2):199–206
Poulin S, Larsen A (2007) Drag loading of circular cylinders inclined in the along-wind direction. J Wind Eng Ind Aerodyn 95(9–11):1350–1363
Poza P et al (2002) Fractographic analysis of silkworm and spider silk. Eng Fract Mech 69(9):1035–1048
Pugno NM (2007) Towards a Spiderman suit: large invisible cables and self-cleaning releasable superadhesive materials. J Phys Condens Matter 19(39):395001
Pugno N (2011) The theory of multiple peeling. Int J Fract 171(2):185–193
Pugno NM, Lepore E (2008) Observation of optimal gecko's adhesion on nanorough surfaces. Biosystems 94(3):218–222
Pugno N et al (2008) Atomistic fracture: QFM vs. MD. Eng Fract Mech 75(7):1794–1803
Pugno N, Cranford SW, Buehler MJ (2013) Synergetic material and structure optimization yields robust spider web anchorages. Small. doi:10.1002/smll.201201343
Rammensee S et al (2008) Assembly mechanism of recombinant spider silk proteins. Proc Natl Acad Sci USA 105(18):6590–6595
Rice JR, Rosengre GF (1968) Plane strain deformation near a crack tip in a power-law hardening material. J Mech Phys Solid 16(1):1
Sahni V et al (2012) Cobweb-weaving spiders produce different attachment discs for locomotion and prey capture. Nat Commun 3(1106):1–7
Sen D, Buehler MJ (2011) Structural hierarchies define toughness and defect-tolerance despite simple and mechanically inferior brittle building blocks. Sci Rep 1(1):35
Sensenig A, Agnarsson I, Blackledge TA (2010) Behavioural and biomaterial coevolution in spider orb webs. J Evol Biol 23(9):1839–1856
Shao ZZ, Vollrath F (1999) The effect of solvents on the contraction and mechanical properties of spider silk. Polymer 40(7):1799–1806
Shao ZZ, Vollrath F (2002) Materials: surprising strength of silkworm silk. Nature 418(6899):741
Spivak D et al (2011) Category theoretic analysis of hierarchical protein materials and social networks. PLoS ONE 6. http://dx.plos.org/10.1371/journal.pone.0023911
Sugita Y, Okamoto Y (1999) Replica exchange molecular dynamics method for protein folding. Chem Phys Lett 314:141–151
Swanson BO et al (2006) Variation in the material properties of spider dragline silk across species. Appl Phys A Mater Sci Process 82(2):213–218
Swanson BO, Blackledge TA, Hayashi CY (2007) Spider capture silk: performance implications of variation in an exceptional biomaterial. J Exp Zool A Ecol Genet Physiol 307A(11):654–666
Swanson BO et al (2009) The evolution of complex biomaterial performance: the case of spider silk. Integr Comp Biol 49(1):21–31
Tang ZY et al (2003) Nanostructured artificial nacre. Nat Mater 2(6):413–418
Tarakanova A, Buehler MJ (2012a) A materiomics approach to spider silk: protein molecules to webs. JOM 64(2):214–225
Tarakanova A, Buehler MJ (2012b) The role of capture spiral silk properties in the diversification of orb webs. J R Soc Interface 9(77):3240–3248
Termonia Y (1994) Molecular modeling of spider silk elasticity. Macromolecules 27(25):7378–7381
Tian Y et al (2006) Adhesion and friction in gecko toe attachment and detachment. Proc Natl Acad Sci USA 103(51):19320–19325
van Beek JD et al (2002) The molecular structure of spider dragline silk: folding and orientation of the protein backbone. Proc Natl Acad Sci USA 99(16):10266–10271

Varenberg M, Pugno NM, Gorb SN (2010) Spatulate structures in biological fibrillar adhesion. Soft Matter 6(14):3269–3272
Vepari C, Kaplan DL (2007) Silk as a biomaterial. Prog Polym Sci 32(8–9):991–1007
Vincent JFV (2001) Stealing ideas from nature. In: Deployable structures. Springer, Vienna, pp 51–58
Vollrath F (1992) Spider webs and silks. Sci Am 266(3):70–76
Vollrath F (1999) Biology of spider silk. Int J Biol Macromol 24:81–88
Vollrath F (2000) Strength and structure of spiders' silks. Rev Mol Biotechnol 74:67–83
Vollrath F (2010) Spider silk: evolution and 400 million years of spinning, waiting, snagging, and mating. Nature 466(7304):319
Vollrath F, Knight DP (2001) Liquid crystalline spinning of spider silk. Nature 410(6828):541–548
Vollrath F, Mohren W (1985) Spiral geometry in the garden spider's orb web. Naturwissenschaften 72(12):666–667
Vollrath F, Porter D (2006) Spider silk as archetypal protein elastomer. Soft Matter 2(5):377–385
Vollrath F, Porter D (2009) Silks as ancient models for modern polymers. Polymer 50(24):5623–5632
Vollrath F, Selden P (2007) The role of behavior in the evolution of spiders, silks, and webs. Annu Rev Ecol Evol Syst 38:819–846
Vollrath F et al (1996) Structural organization of spider silk. Proc R Soc Lond B Biol Sci 263(1367):147–151
Vollrath F, Porter D, Holland C (2011) There are many more lessons still to be learned from spider silks. Soft Matter 7(20):9595–9600
Zschokke S, Vollrath F (1995) Web construction patterns in a range of orb-weaving spiders (Araneae). Eur J Entomol 92(3):523–541